INSTITUTE
FOR
AEROSPACE STUDIES

UNIVERSITY OF TORONTO

CHARACTERISTICS OF THE MEAN WIND AND TURBULENCE IN THE PLANETARY BOUNDARY LAYER

by

H. W. Teunissen

October, 1970.

UTIAS Review No. 32

CHARACTERISTICS OF THE MEAN WIND AND TURBULENCE IN THE PLANETARY BOUNDARY LAYER

by

H. W. Teunissen

Manuscript received August 1970

October, 1970. UTIAS Review No.32

ACKNOWLEDGEMENT

The author wishes to thank Professor B. Etkin as well as his fellow students for their assistance in the form of many stimulating and informative discussions carried on throughout this review. In addition, thanks are expressed to the library staff of UTIAS for their assistance in obtaining the reference material necessary to carry out the investigation.

Financial support for this work has been received from the United States Air Force, Flight Dynamics Laboratory, Wright-Patterson Air Force Base, under contract No. ~~F33615-C-1055~~ F33615-68-C-1055, and from the National Research Council of Canada.

SUMMARY

Considerable information is available to date concerning the characteristics of the flow in the planetary boundary layer, which comprises roughly the lowest two thousand feet of the atmosphere. Unfortunately, in many instances, the results from different sources do not always agree. This is in part due to the extremely complex nature of the flow and as a result, some confusion exists as to the exact description of the planetary layer. For this reason, a fairly extensive survey of the existing data has been carried out, and the results of this review are presented herein. The planetary layer is described in detail with respect to both mean velocity and turbulence, and the effect of thermal stability and surface conditions on these characteristics is discussed. Finally, a simplified analytical representation of the flow in the planetary layer is presented.

BLANK PAGE

TABLE OF CONTENTS

		PAGE
	Acknowledgements	
	Summary	
	Notation	
I.	INTRODUCTION	1
II.	DEFINITIONS AND THEORY OF TURBULENCE	1
	2.1 Correlations	1
	2.2 Integral Scales	5
	2.3 Taylor's Hypothesis	5
	2.4 Spectral Density Functions	6
	2.5 Homogeneity and Isotropy	10
III.	CHARACTERISTICS OF THE PLANETARY BOUNDARY LAYER	12
	3.1 General Description	12
	3.2 Atmospheric Stability	13
	3.3 Simplifying Assumptions	14
	3.3.1 Stationarity	14
	3.3.2 Homogeneity	14
	3.3.3 Isotropy	14
	3.3.4 Taylor's Hypothesis	16
	3.4 Mean Wind Characteristics	17
	3.4.1 Velocity Profiles	17
	3.4.2 Mean Wind Direction	18
	3.5 Reynolds Stresses	19
	3.5.1 Total Kinetic Energy of Turbulence	19
	3.5.2 Vertical Component Variance	20
	3.5.3 Lateral Component Variance	20
	3.5.4 Longitudinal Component Variance	21
	3.5.5 Summary of Variances	21
	3.5.6 Other Reynolds Stresses	22
	3.6 One-Dimensional Spectral Density Functions	23
	3.6.1 Vertical Component Spectrum	23
	3.6.2 Lateral Component Spectrum	25
	3.6.3 Longitudinal Component Spectrum	26
	3.6.3.1 Total Velocity Spectrum	26
	3.6.3.2 Gust Velocity Spectrum	27
	3.6.4 Cross-Spectra	29
	3.6.5 Cross-Correlation Spectrum	31

3.7 Integral Scales of Turbulence 34

IV. MATHEMATIC MODEL OF THE PLANETARY BOUNDARY LAYER 39

4.1 Assumptions 39
4.2 Mean Velocity Profile 39
4.3 Reynolds Stresses 40
4.4 Power Spectra 40
4.5 Cross-Spectra 41
4.6 Integral Scales 41

REFERENCES 42

NOTATION

A, B, C	constants relating fluctuating component variances to friction velocity (Sec. 3.5)
a, c, c_z, c_{10}	constants used in cross-correlation spectrum expressions (Sec. 3.6.5)
$C_{ij}(n)$	co-spectral density function (Sec. 2.4)
$E_{ij}(\underline{k}, n)$	four-dimensional spectral density tensor (Sec. 2.4)
$\bar{e}$	total mean turbulent kinetic energy
f	$\equiv k.z$
$f_p^{\cdot i}$	$\equiv k_p^{\cdot i}.z$
$f(r)$, $f_u(r_x)$, etc.	longitudinal correlation coefficients (Sec. 2.1 and 2.5)
g	gravitational acceleration
$g(r)$, $g_v(r_x)$, etc.	lateral correlation coefficients (Sec. 2.1 and 2.5)
$\underline{i}$	unit vector in x-direction
i	$\equiv \sqrt{-1}$; also, an index referring to u, v, or w
$\underline{j}$	unit vector in y-direction
j	an index referring to u, v, or w
K	von Kármán's constant ≈ 0.4
K_m	eddy viscosity
k	reduced frequency or wave number $\equiv n/\bar{U}$ cycles per foot
$k_p^{\cdot i}$	value of k at maximum value of the non-dimensionalized spectrum of the 'i' velocity component
$\underline{k}$	wave number vector $\equiv \underline{i}\, k_x + \underline{j} k_y + \underline{k}\, k_z$; also, unit vector in z -direction
k	$\lvert \underline{k} \rvert$
ℓ	Prandtl mixing length
L	length scale defined by Davenport and Harris (Secs. 3.6.5 and 3.7)
L'	scaling length defined by $\dfrac{\bar{U}_\tau\, (\partial \bar{U}/\partial z) T}{Kg(\partial \theta/\partial z)}$
$L_i^{\,x}, L_i^{\,y}, L_i^{\,z}, L_u, L_v$	integral length scales of turbulence (Sec. 2.2 and 2.5)
n, n'	frequencies, cycles per second

p	pressure
$Q_{ij}(n)$	quadrature spectrum (Sec. 2.4)
$\underline{r}$	spatial separation vector $\equiv \underline{i}\, r_x + \underline{j}\, r_y + \underline{k}\, r_z$; $\lvert\underline{r}\rvert \equiv r$
Ri	gradient Richardson Number (Sec.3.2)
$R_{ij}(r_x,r_y,r_z,\tau)$	general double velocity correlation tensor (Sec. 2.1)
$R_{ij}, R_{ij}(r_x)$, etc.	one-dimensional correlation tensors (Sec. 2.1)
$\mathcal{R}_{ij}(\tau)$	Eulerian time-delay correlation tensor (Sec. 2.1)
t	time
T	temperature
T_i^x	integral time scale of turbulence (Sec. 2.2)
$U(t)$	total velocity component in x-direction $\equiv \bar{U} + u(t)$
$\bar{U}$	mean velocity in x-direction
$\underline{U}(t)$	turbulence velocity vector $\equiv \underline{i}\, u(t) + \underline{j} v(t) + \underline{k}\, w(t)$
$\bar{U}_\tau$	friction velocity
$\bar{U}_G$	gradient wind velocity (Sec. 3.1)
$u(t)$, $v(t)$, $w(t)$	fluctuating velocity components in x, y and z directions, respectively
u', v', w'	rms values of fluctuating velocity components; $u' \equiv \sqrt{\overline{u^2}}$, $v' \equiv \sqrt{\overline{v^2}}$, $w' \equiv \sqrt{\overline{w^2}}$
x, y, z	Cartesian coordinate axes
z	height above earth's surface
z_o	roughness length (Sec. 3.4)
z_G	gradient height (Sec. 3.1)
α	mean velocity power law index (Sec. 3.4); also, angle between mean wind and geostropic direction
γ	lapse rate $\equiv -dT/dz$
γ_o	constant defined in Sec. 3.6.4
$\gamma_{ij}^2(n)$	coherence function (Sec. 2.4)
$\gamma_{ij}(k,y_1,y_2), \gamma_{ij}(k,r_y)$	magnitude of cross-correlation spectrum (Sec.3.6.5)
Γ	dry adiabatic lapse rate $\approx 1^\circ$C/100 m $\approx 5.5^\circ$F/1000 ft.
λ	wavelength $\equiv 1/k = \bar{U}/n$, feet

ρ	air density
θ	potential temperature ≡ temperature which a volume of air assumes when brought adiabatically from its existing pressure to that at the earth's surface
$\phi_{ij}(n), \phi_{ij}(k_x)$, etc.	one-dimensional spectral density functions (Sec. 2.4)
$\Phi_{ij}(k), \Phi'_{ij}(\omega), \Phi''_{ij}(\Omega)$	one-dimensional spectral density functions (Eq. (29))
$\Phi_{\bar{U}}(k)$	power spectrum of total velocity component in x-direction
Ψ_{ij}	function related to cross-correlation spectrum (Sec. 3.6.5)
τ	incremental time-delay; also shear stress
τ_o	surface shear stress
ω	frequency, radians per second, ≡ $2\pi n$
Ω	reduced frequency, radians per foot, ≡ $2\pi k$
$\tilde{a}$	non-dimensional form of a
$\bar{a}$	time average of a

BLANK PAGE

I. INTRODUCTION

In the past few years, it has been increasingly important to know in detail the characteristics of the atmosphere at low altitudes. The present emphasis on low-flying and V/STOL aircraft is in part responsible for this requirement, as is the advent of rocketry, with its large launch vehicles. In addition, the continuation of the trend toward taller and more radically shaped buildings and structures necessitates a good simulation of the flows at these levels in order realistically to determine their response to these flows. The prominence of the pollution control issue in recent years has also added weight to the requirement of achieving a proper description, and ultimately simulation of the planetary boundary layer.

To date, considerable data has been gathered in both the aeronautical and meteorological disciplines. While the information is by no means complete, it is possible to draw many conclusions about the nature of the planetary layer, and in particular the turbulence therein. Due to the extremely complex nature of the flows, however, there is sometimes considerable variability in the conclusions that have been drawn. For example, there have been widely scattered conclusions about the magnitude and variation of the integral scales of turbulence through the planetary layer. This has been due in part to a lack of rigor in determining exactly what scales are being obtained in some cases, and in part to the refusal of the atmosphere to submit easily to simple descriptions.

It is the purpose of this review to describe and summarize most of the existing data on the characteristics of the flows in the planetary layer, and to attempt to clarify some of the discrepancies that have occurred in the past. In addition, in light of the data available, a simplified mathematical model is suggested to represent the flows.

II. DEFINITIONS AND THEORY OF TURBULENCE

In the literature on turbulence there is on the whole a fairly wide range of notation used. In order to avoid confusion and to clarify precisely what is being referred to in this review, the notation and definitions of turbulence theory used in this report are presented in some detail in the following pages.

2.1 Correlations

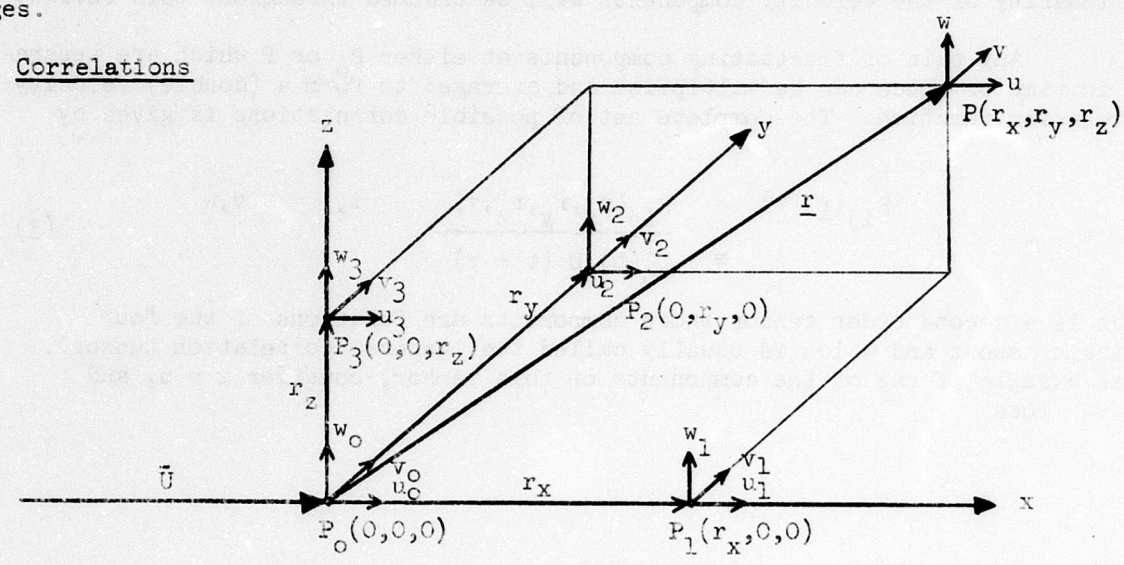

Consider the two arbitrary points P_o and P separated by a vector $\underline{r} = \underline{i}\, r_x + \underline{j}\, r_y + \underline{k}\, r_z$ in a homogenous three-dimensional turbulence field as shown above. Let the flow be moving with mean velocity $\bar{U}$ along the x-axis of a fixed Eulerian reference frame of which P_o is the origin. The points P_1, P_2 and P_3 are the projections of P on the coordinate axes. The turbulent motion at any point in the field is represented by the vector $\underline{U}(t) = \underline{i}u(t) + \underline{j}v(t) + \underline{k}w(t)$, with appropriate subscripts, where u(t), v(t) and w(t) are the longitudinal, lateral and vertical fluctuating velocity components, respectively. Thus the total (Eulerian) velocity in the x-direction at P_o is

$$U_o(t) = \bar{U}(t_1, T) + u_o(t)$$

where $\bar{U}(t_1, T)$ is the mean velocity and is defined by

$$\bar{U}(t_1, T) \equiv \frac{1}{2T} \int_{t_1-T}^{t_1+T} U_o(t)\, dt \tag{1}$$

and is the same at all points in the field due to the assumption of homogeneity. The mean of the fluctuating component $u_o(t)$ as defined by Eq. (1) is necessarily zero, as it is for the other two components $v_o(t)$ and $w_o(t)$ at P_o since there is mean motion only in the x-direction, and similarly for any other points in the field. The three fluctuating components, in addition to $U_o(t)$, are random functions of time, and as such are said to be stationary if their statistical properties are independent of time in the limit as $T \to \infty$. Thus for stationary flow, $\bar{U}(t_1, T)$ is independent of t_1 and the mean velocity is given by

$$\bar{U} = \lim_{T\to\infty} \frac{1}{2T} \int_{-T}^{T} U_o(t)\, dt \tag{2}$$

and thus

$$U_o(t) = \bar{U} + u_o(t).$$

Stationarity of the velocity components will be assumed throughout this review.

Any pair of fluctuating components at either P_o or P which are separated in time or space can be multiplied and averaged to form a (double) velocity correlation function. The complete set of possible correlations is given by

$$\begin{aligned} R_{ij}(\underline{r}, \tau) &= \frac{R_{ij}(r_x, r_y, r_z, \tau)}{} \qquad i,j = u,v,w \\ &\equiv \underline{U}_o^T(t)\, \underline{U}\,(t + \tau) \end{aligned} \tag{3}$$

which is a second order tensor whose components are functions of the four variables shown and which is usually called the 'general correlation tensor'. As an example of one of the components of this tensor, consider i = u, and j = v. Then

$$R_{uv}(r_x, r_y, r_z, \tau) \equiv \overline{u_o(t)\, v(t+\tau)}$$

$$= \lim_{T\to\infty} \frac{1}{2T} \int_{-T}^{T} u_o(t)\, v(t+\tau)\, dt$$

$$= \lim_{T\to\infty} \frac{1}{2T} \int_{-T}^{T} u(0,0,0,t)\, v(r_x, r_y, r_z, t+\tau)\, dt \qquad (4)$$

since $u_o(t)$ is the component at P_o and $v(t)$ is at P.

It should be noted that in defining the mean velocity and correlations above, time averages of the velocity signals have been used, since it is these averages that are actually measured in practice. However, it may in some cases be mathematically advantageous to consider ensemble averages rather than time averages. For example, if $U_K(t)$ represents an ensemble of N records of the velocity U(t) where K = 1,...N, then the ensemble average of U(t) is defined by

$$\bar{U} \equiv \lim_{N\to\infty} \sum_{K=1}^{N} U_K(t_1)$$

where U(t) is assumed stationary such that U is independent of the arbitrary point in time, t_1. In the special case when the time-averaged mean velocity as defined by Eq. (2), as well as any other statistical properties of U(t), are identical regardless of which of the K records of U(t) is used in obtaining them, U(t) is said to be ergodic. In this case, time averages are equivalent to ensemble averages such that the mean velocity as defined by Eq. (2) is identical to the ensemble average defined above. In practice, ergodicity of the velocities is usually assumed. Note also that ergodicity requires stationarity, but not vice-versa.

Of the general correlation tensor of Eq. (3), we are particularly interested in five special cases. These are

$$R_{ij}(r_x,0,0,0),\ R_{ij}(0,r_y,0,0),\ R_{ij}(0,0,r_z,0),$$
$$R_{ij}(0,0,0,0) \quad \text{and} \quad R_{ij}(r_x,0,0,\tau).$$

The first three of these special tensors are zero time-delay spatial cross-correlations between the turbulence components at P_o and those at P_1, P_2 and P_3, respectively, as shown in the above sketch. They are given typically by

$$R_{ij}(r_x,0,0,0) \equiv \begin{bmatrix} \overline{u_o(t)u_1(t)} & \overline{u_o(t)v_1(t)} & \overline{u_o(t)w_1(t)} \\ \overline{v_o(t)u_1(t)} & \overline{v_o(t)v_1(t)} & \overline{v_o(t)w_1(t)} \\ \overline{w_o(t)u_1(t)} & \overline{w_o(t)v_1(t)} & \overline{w_o(t)w_1(t)} \end{bmatrix} \equiv R_{ij}(r_x) \qquad (5)$$

and similarly,

$$R_{ij}(0,r_y,0,0) \equiv R_{ij}(r_y)$$
and
$$R_{ij}(0,0,r_z,0) \equiv R_{ij}(r_z). \qquad (6)$$

The fourth tensor is the well-known Reynolds Stress tensor and is given by

$$R_{ij}(0,0,0,0) \equiv \begin{bmatrix} \overline{u_o^2(t)} & \overline{u_o(t)v_o(t)} & \overline{u_o(t)w_o(t)} \\ \overline{v_o(t)u_o(t)} & \overline{v_o^2(t)} & \overline{v_o(t)w_o(t)} \\ \overline{w_o(t)u_o(t)} & \overline{w_o(t)v_o(t)} & \overline{w_o^2(t)} \end{bmatrix} \equiv R_{ij}. \qquad (7)$$

The diagonal components of this tensor are of course the familiar mean-square values of the velocity components. The root-mean-square (rms) values or variances $\sqrt{\overline{u_o^2}}$, $\sqrt{\overline{v_o^2}}$ and $\sqrt{\overline{w_o^2}}$ are rewritten as u_o', v_o' and w_o', respectively, for simplicity. Finally, the fifth special tensor is important because it in fact represents the single point time-delay correlations that are measured by a probe at a fixed point such as P_o in a laboratory (Eulerian) frame. That is, in a time increment τ, the mean flow moves along the x-axis a distance $\bar{U}\tau$ and if we simply set $r_x = \bar{U}\tau$, we obtain

$$R_{ij}(r_x,0,0,\tau) = R_{ij}(\bar{U}\tau,0,0,\tau) \equiv \mathcal{R}_{ij}(\tau) \qquad (8)$$

where

$$\mathcal{R}_{ij}(\tau) \equiv \begin{bmatrix} \overline{u_o(t)u_o(t+\tau)} & \overline{u_o(t)v_o(t+\tau)} & \overline{u_o(t)w_o(t+\tau)} \\ \overline{v_o(t)u_o(t+\tau)} & \overline{v_o(t)v_o(t+\tau)} & \overline{v_o(t)w_o(t+\tau)} \\ \overline{w_o(t)u_o(t+\tau)} & \overline{w_o(t)v_o(t+\tau)} & \overline{w_o(t)w_o(t+\tau)} \end{bmatrix} \qquad (9)$$

and is obtained by correlating time-delayed signals as measured by a probe fixed at P_o. The diagonal components of this tensor are called 'autocorrelations' since the components are being correlated with themselves. It is also to be noted that from Eq.(8) for $\tau = 0$, $\mathcal{R}_{ij}(\tau)$ may be related to the Reynolds Stress tensor of Eq.(7); that is $\mathcal{R}_{ij}(0) = R_{ij}$.

Generally, the various correlation functions defined above are normalized to yield correlation coefficients. This normalization is done using the appropriate rms values of the velocity components such that, for example, the normalized form of the u-v correlation function defined in Eq.(4) is

$$\tilde{R}_{uv}(r_x,r_y,r_z,\tau) \equiv \frac{R_{uv}(r_x,r_y,r_z,\tau)}{u'\,v'}$$

and similarly for any of the other correlations. The only exceptions to this rule are the three diagonal components of the Reynolds Stress tensor. Since these components are themselves the mean-square values of the velocities, normalization as above necessarily yields unity and is therefore of no use. For this reason, the roots of these components are simply non-dimensionalized either by the friction velocity $\bar{U}_\tau$, or by the mean velocity $\bar{U}$ in which case the familiar turbulence intensities given by $u_o'/\bar{U}$, $v_o'/\bar{U}$ and $w_o'/\bar{U}$ are obtained.

In general, the diagonal components of the spatial correlation coefficient tensors are referred to as either 'longitudinal' or 'lateral' correlation coefficients. This nomenclature derives from the direction of the velocity component being correlated at the two points with respect to the vector $\underline{r}$ separating the points. If the component is parallel to this vector, the correlation is called longitudinal and the function f(r) is used to denote the

coefficient, where

$$r = |\underline{r}| = \sqrt{r_x^2 + r_y^2 + r_z^2} \quad ;$$

if it is perpendicular to $\underline{r}$, the correlation is called lateral and the function $g(r)$ denotes the coefficient. Thus there are three longitudinal correlation coefficients given by

$$\begin{aligned} f_u(r_x) &\equiv \tilde{R}_{uu}(r_x), \\ f_v(r_y) &\equiv \tilde{R}_{vv}(r_y), \\ \text{and} \quad f_w(r_z) &\equiv \tilde{R}_{ww}(r_z), \end{aligned} \tag{10}$$

and six lateral coefficients given typically by

$$g_v(r_x) \equiv \tilde{R}_{vv}(r_x), \; g_w(r_x) = \tilde{R}_{ww}(r_x), \tag{11}$$

and similarly for $g_u(r_y)$, $g_w(r_y)$, $g_u(r_z)$ and $g_v(r_z)$.

2.2 Integral Scales

An integral or 'macro-scale' of turbulence can be defined for any correlation coefficient of any of the special tensors defined in the previous section except the Reynolds Stress tensor. The scale is defined as the integral of the correlation coefficient over the positive range of its independent variable, and it can thus be either a length scale or a time scale. One can therefore define four scale tensors corresponding to the four tensors $R_{ij}(r_x)$, $\tilde{R}_{ij}(r_y)$, $\tilde{R}_{ij}(r_z)$ and $\tilde{\mathcal{R}}_{ij}(\tau)$. However, only the diagonal components of these tensors are of major interest, and in the case of the first three tensors, one obtains nine scale lengths defined by

$$L_i^x \equiv \int_o^\infty \tilde{R}_{ii}(r_x)dr_x, \tag{a}$$

$$L_i^y \equiv \int_o^\infty \tilde{R}_{ii}(r_y)dr_y, \tag{b}$$

and

$$L_i^z \equiv \int_o^\infty \tilde{R}_{ii}(r_z)dr_z, \; i = u,v,w. \tag{c}$$

From the $\tilde{\mathcal{R}}_{ij}(\tau)$ tensor, the three time scales of importance are given by

$$T_i^x \equiv \int_o^\infty \tilde{\mathcal{R}}_{ii}(\tau)\, d\tau \tag{13}$$

and these time scales can be related to the length scales L_i^x through the use of Taylor's Hypothesis (see below).

As with the correlation coefficients of Eqs.(10) and (11), the length scales of Eqs.(12) are referred to as longitudinal or lateral scales, the criterion logically being from which type of correlation coefficient they are obtained. Thus from these equations it is seen that L_u^x, L_v^y and L_w^z are longitudinal scales, while the other six scales of Eqs.(12) are lateral scales.

2.3 Taylor's Hypothesis

Taylor's Hypothesis provides a time-space transformation which allows spatial variations in the turbulence field to be expressed in terms of time

variations at a fixed point in the field. The hypothesis states that in a Lagrangian reference frame moving with the mean flow, there is no time variation of the components - that is, the field is 'frozen'. Mathematically, this may be stated as

$$\partial/\partial t = -\bar{U}\partial/\partial x \tag{14}$$

and the hypothesis is made under the assumption that $\bar{U} >> u'$. The physical interpretation of this is that the time fluctuations at a fixed point in the field such as P_o can be imagined to be caused solely by the entire field being frozen at a particular instant and convected past the point with the constant velocity $\bar{U}$. The velocity fluctuations over a period of time at the point will then be identical with the instantaneous distribution of the velocity $u_o(t)$ along the x-axis through the point. These physical implications will be further discussed in the following section.

In terms of the previously defined correlations, Taylor's Hypothesis means that $R_{ij}(\underline{r},\tau)$ is now replaced by $R_{ij}(\underline{r})$. Thus the time-delay correlation of Eq.(8) may now be written

$$\mathcal{R}_{ij}(\tau) = R_{ij}(r_x,0,0)$$

which is identical to the spatial cross-correlation $R_{ij}(r_x)$ of Eq.(5). Thus we may now write

$$\mathcal{R}_{ij}(\tau) = R_{ij}(r_x)$$

or

$$\tilde{\mathcal{R}}_{ij}(\tau) = \tilde{R}_{ij}(r_x), \quad r_x = \bar{U}\tau \tag{15}$$

and $R_{ij}(r_x)$ may be determined simply by measuring the velocity signals at a fixed point and obtaining the time-delay correlations of these signals. Using this result and Eqs.(12a) and (13), it is now possible to relate the scales L_i^x and T_i^x. That is,

$$L_i^x = \int_o^\infty \tilde{R}_{ii}(r_x)dr_x = \int_o^\infty \tilde{\mathcal{R}}_{ii}(\tau)\, d(\bar{U}\tau) = \bar{U}T_i^x \tag{16}$$

Strictly speaking, Taylor's Hypothesis was made for homogeneous, isotropic turbulence, although it has been found quite reasonable for non-isotropic uniform flows. Its application in shear flows, however, requires further consideration (see Sec. 3.3.4).

2.4 Spectral Density Functions

Associated with any correlation function is a corresponding spectrum function defined as the Fourier Transform of the correlation. Thus for the general correlation tensor of Eq.(3), one obtains a tensor of spectra given by

$$E_{ij}(\underline{k},n') \equiv 16 \iiint_{-\infty}^{\infty} R_{ij}(\underline{r},\tau)e^{-i2\pi(\underline{k}\cdot\underline{r} + n'\tau)}\, d\underline{r}\, d\tau \tag{17}$$

where $\underline{k} = \underline{i}\, k_x + \underline{j}\, k_y = \underline{k}\, k_z$ is the wave number vector corresponding to the separation vector $\underline{r}$ after the transformation. Writing Eq.(17) out in full gives

$$E_{ij}(k_x,k_y,k_z,n') \equiv 16 \iiint_{-\infty}^{\infty} R_{ij}(r_x,r_y,r_z,\tau)e^{-i2\pi(k_x r_x + k_y r_y + k_z r_z + n'\tau)}\, dr_x dr_y dr_z d\tau. \tag{18}$$

The tensor $E_{ij}(\underline{k},n')$ is a tensor of four-dimensional spectrum functions and can of course be used to regain the correlation tensor through the inverse Fourier Transform such that

$$R_{ij}(\underline{r},\tau) = \frac{1}{16} \iiiint_{-\infty}^{\infty} E_{ij}(\underline{k},n') e^{i2\pi(\underline{k}.\underline{r} + n'\tau)} \, d\underline{k}dn'.$$

Suppose now that we insert in the above equations the relation $r_x = \bar{U}\tau$ which was used to relate r_x and τ in the previous section. Then Eq.(18) becomes

$$E_{ij}[(k_x + n'/\bar{U}),k_y,k_z] = 8 \iiint_{-\infty}^{\infty} R_{ij}(r_x,r_y,r_z) e^{-i2\pi[(k_x+n'/\bar{U})r_x+k_y r_y+k_z r_z]} \, dr_x dr_y dr_z.$$

Now let $n = k_x\bar{U} + n'$. Physically, the frequency n represents the overall time fluctuations as seen by an observer at a fixed point such as P_o while the flow sweeps by with mean velocity $\bar{U}$ relative to the point. It is therefore the frequency which would be measured in an experiment by a probe fixed at P_o, and is the sum of the two frequencies n' and $k_x\bar{U}$. The frequency n' is that which would be seen by the observer at a fixed point in a Lagrangian frame moving with the fluid. In this case, the relative velocity between the observer and the flow would be zero such that n = n'. The remaining frequency $k_x\bar{U}$ represents the time fluctuations that are due entirely to the flow field being convected past P_o with the relative mean velocity $\bar{U}$. In fact, if $\bar{U}$ is large enough such that $k_x\bar{U} \gg n'$, then $n \approx k_x\bar{U}$ and this is none other than Taylor's Hypothesis. That is, if the flow were truly 'frozen', n' would be zero and $n = k_x\bar{U}$. Thus it can be seen that the validity of Taylor's Hypothesis depends on the relative velocity between the observer and the flow field, and if this velocity is very small such that n' is of the order of $k_x\bar{U}$, then n' cannot be neglected with respect to $k_x\bar{U}$ and the frozen flow hypothesis is not valid. Skelton (Ref.6) suggests that the minimum relative velocity for the hypothesis to be valid is about one-third of the mean flow velocity.

Returning now to the spectrum tensor, we may write

$$E_{ij}(n/\bar{U},k_y,k_z) = 8 \iiint_{-\infty}^{\infty} R_{ij}(r_x,r_y,r_z) e^{-i2\pi[(n/\bar{U})r_x+k_y r_y+k_z r_z]} \, dr_x dr_y dr_z$$

and if Taylor's Hypothesis is assumed (n' = 0), $n = k_x\bar{U}$ and E_{ij} may be written

$$E_{ij}(k_x,k_y,k_z) = 8 \iiint_{-\infty}^{\infty} R_{ij}(r_x,r_y,r_z) e^{-i2\pi(k_x r_x + k_y r_y + k_z r_z)} \, dr_x dr_y dr_z. \qquad (19)$$

Consider now the special tensors defined by Eqs.(5), (6) and (9). By Fourier transforming these one-dimensional correlations, one can define the corresponding one-dimensional spectrum functions by

$$\phi_{ij}(k_x) \equiv 2 \int_{-\infty}^{\infty} R_{ij}(r_x) \, e^{-i2\pi k_x r_x} \, dr_x \qquad (a)$$

$$\phi_{ij}(k_y) \equiv 2\int_{-\infty}^{\infty} R_{ij}(r_y)\, e^{-i2\pi k_y r_y}\, dr_y \qquad (b) \qquad (20)$$

$$\phi_{ij}(k_z) \equiv 2\int_{-\infty}^{\infty} R_{ij}(r_z)\, e^{-i2\pi k_z r_z}\, dr_z \qquad (c)$$

and

$$\Phi_{ij}(n) \equiv 2\int_{-\infty}^{\infty} \mathcal{R}_{ij}(\tau)\, e^{-i2\pi n\tau}\, d\tau. \qquad (21)$$

The corresponding inverse transforms are of course

$$R_{ij}(r_x) \equiv \tfrac{1}{2}\int_{-\infty}^{\infty} \phi_{ij}(k_x) e^{i2\pi k_x r_x}\, dk_x \qquad (a)$$

$$R_{ij}(r_y) \equiv \tfrac{1}{2}\int_{-\infty}^{\infty} \phi_{ij}(k_y) e^{i2\pi k_y r_y}\, dk_y \qquad (b) \qquad (22)$$

$$R_{ij}(r_z) \equiv \tfrac{1}{2}\int_{-\infty}^{\infty} \phi_{ij}(k_z) e^{i2\pi k_z r_z}\, dk_z \qquad (c)$$

and

$$\mathcal{R}_{ij}(\tau) \equiv \tfrac{1}{2}\int_{-\infty}^{\infty} \Phi_{ij}(n) e^{i2\pi n\tau}\, dn. \qquad (23)$$

The $\Phi_{ij}(n)$ spectra of Eq.(21) are those which are obtained by placing a measuring instrument at a fixed point in the flow, and if Taylor's Hypothesis is assumed, these can be easily related to the $\phi_{ij}(k_x)$ spectra. That is, from Eqs.(15) and (20a), and since $r_x = \bar{U}\tau$ and $k_x = n/\bar{U}$,

$$\phi_{ij}(k_x) = 2\int_{-\infty}^{\infty} R_{ij}(r_x) e^{-i2\pi k_x r_x}\, dr_x$$

$$= 2\,\bar{U}\int_{-\infty}^{\infty} \mathcal{R}_{ij}(\tau)\, e^{-i2\pi n\tau}\, d\tau.$$

Comparing this with Eq. (21), it can therefore be seen that

$$\phi_{ij}(k_x) = \bar{U}\,\Phi_{ij}(n).$$

Notice also that in the particular case of $\tau = 0$, Eq.(23) may be used to relate the Reynolds Stress tensor to the $\Phi_{ij}(n)$ tensor by

$$\mathcal{R}_{ij}(0) = R_{ij} = \tfrac{1}{2}\int_{-\infty}^{\infty} \Phi_{ij}(n)\, dn. \qquad (24)$$

The one-dimensional spectra defined by Eqs.(20) could also have been obtained by integration of the three-dimensional spectra of Eq.(19). For example, $\phi_{ij}(k_x)$ is also given by the double integration of $E_{ij}(k_x,k_y,k_z)$ over k_y and k_z. Similarly, two-dimensional spectra can be defined by integrating E_{ij} over only one variable, but these will not be dealt with here.

As with the correlation functions and integral scales of turbulence, special terminology is generally applied to the spectrum functions. Of the nine

diagonal components of the tensors defined by Eqs. (20), three are termed longitudinal spectra and the other six lateral spectra, depending on whether longitudinal or lateral correlations appear in their definition. In addition, the diagonal components of Eqs. (20) and (21), which are defined by autocorrelation functions, are usually called 'power spectral densities' or 'power spectra' while the off-diagonal components are referred to as 'cross-spectral densities' or simply 'cross-spectra'. Since the spectra of the $\phi_{ij}(n)$ tensor are those that are measured in practice, they are of the most interest and unless specified otherwise, the terms 'power-spectra' and 'cross-spectra' refer to these spectra throughout the remainder of this review.

Because of the assumption of stationarity, the power spectra $\phi_{ii}(n)$ are even functions of the frequency n. Thus from Eqs. (21) and (23),

$$\phi_{ii}(n) = 4 \int_0^\infty \mathcal{R}_{ii}(\tau) \cos(2\pi n\tau) d\tau \tag{25}$$

and

$$\mathcal{R}_{ii}(\tau) = \int_0^\infty \phi_{ii}(n) \cos(2\pi n\tau)\, dn. \tag{26}$$

In particular, for $\tau = 0$, one obtains from Eq. (26) the expressions

$$\mathcal{R}_{uu}(0) \equiv \overline{u^2} = \int_0^\infty \phi_{uu}(n)\, dn \qquad \text{(a)}$$

$$\mathcal{R}_{vv}(0) \equiv \overline{v^2} = \int_0^\infty \phi_{vv}(n)\, dn \qquad \text{(b)} \tag{27}$$

$$\mathcal{R}_{ww}(0) \equiv \overline{w^2} = \int_0^\infty \phi_{ww}(n)\, dn \qquad \text{(c)}$$

indicating that the area under the power spectrum of any velocity component is equal to the mean square of the component. Equation (25) shows that the power spectra are real functions of n. The cross-spectra, however, are complex functions of n, with

$$\phi_{ij}(-n) = \phi_{ij}^*(n) \equiv \phi_{ji}(n), \quad i \neq j.$$

These spectra are generally redefined as

$$\phi_{ij}(n) \equiv 2 \int_{-\infty}^\infty \mathcal{R}_{ij}(\tau)\, e^{-i2\pi n\tau}\, d\tau$$

$$\equiv C_{ij}(n) - i\, Q_{ij}(n), \quad i \neq j$$

where $C_{ij}(n)$ is called the co-spectral density or co-spectrum and $Q_{ij}(n)$ is called the quad-spectrum, and these functions are real-valued even and odd functions of n, respectively. In addition, these cross-spectra can be expressed in coefficient form by the coherence function, defined by

$$\gamma_{ij}^2(n) \equiv \frac{|\phi_{ij}(n)|^2}{\phi_{ii}(n)\phi_{jj}(n)}, \quad i \neq j \tag{28}$$

where γ_{ij}^2 is the coherence.

Finally, it should be mentioned that in the spectral theory of turbulence, the independent frequency variable n is not always used. In the literature, any of the variables

$$k = n/\bar{U},\ \omega = 2\pi n, \quad \text{or} \quad \Omega = 2\pi n/\bar{U} = 2\pi k$$

may be found where, of course, if Taylor's Hypothesis is assumed, $k \equiv k_x$. In these cases, it is generally Eq. (24) that is used to properly relate the various spectral functions to each other. That is

$$R_{ij} = \tfrac{1}{2}\int_{-\infty}^{\infty} \phi_{ij}(n)dn \equiv \tfrac{1}{2}\int_{-\infty}^{\infty} \Phi_{ij}(k)\, dk$$

$$\equiv \tfrac{1}{2}\int_{-\infty}^{\infty} \Phi_{ij}'(\omega)\, d\omega \equiv \tfrac{1}{2}\int_{-\infty}^{\infty} \Phi_{ij}''(\Omega)\, d\Omega$$

which, along with the above definitions of the independent variables, can be used to show that

$$\Phi_{ij}(k) = \bar{U}\,\phi_{ij}(n) = 2\pi\bar{U}\,\Phi_{ij}'(\omega) = 2\pi\Phi_{ij}''(\Omega) \qquad (29)$$

In the description of the planetary layer which follows, it is the function $\Phi_{ij}(k)$ which will be used. This is because if the 'reduced frequency' or inverse wavelength $k = n/\bar{U}$ is used as the independent variable, where $\bar{U}$ is the mean speed relative to the measuring system, the turbulence measured will not depend on the motion of this system, and spectra measured by aircraft may be directly compared with those obtained on towers (at the same altitude, of course). Note also from Eq. (29) that

$$k\,\Phi_{ij}(k) \equiv n\ \phi_{ij}(n).$$

2.5 Homogeneity and Isotropy

The turbulence field under consideration in the preceding discussion was assumed to be homogeneous. That is, its statistical properties do not vary from point to point in the field, and thus all the functions described are independent of the location of the point P_o in the field. In addition, the assumption of homogeneity allowed the correlations of Sec. 2.1 to be written as functions of the separation between the points rather than of the points themselves, and thus simplified the description considerably.

The concept of isotropy simplifies the description of the turbulence even further. If a turbulence field is isotropic, its statistical properties are independent of direction in the field, and thus they do not change with a rotation of the coordinates axes. Thus isotropy implies homogeneity, but not vice-versa. All off-diagonal components of the special correlation tensors of Sec. 2.1 are zero, as are the corresponding cross-spectra of Sec. 2.4 (note that the off-diagonal components of the general correlation tensor of Eq.(4) are not necessarily zero). All longitudinal correlations are equal, such that

$$f_u(r_x) = f_v(r_y) = f_w(r_z) \equiv f(r) \qquad (30)$$

and all lateral correlations are equal, or

$$g_v(r_x) = g_w(r_x) = g_u(r_y) = g_w(r_y) = g_u(r_z) = g_v(r_z) \equiv g(r) \qquad (31)$$

and the equation of continuity can be used to relate these correlations by

$$g(r) = f(r) + \frac{r}{2} \frac{\partial f(r)}{\partial r} \tag{32}$$

where $r = |\underline{r}|$. Thus only one independent non-zero correlation remains. In addition, Batchelor (Ref.7) has shown that in isotropic turbulence, the general (spatial) correlation tensor is given in terms of $f(r)$ and $g(r)$ by

$$\tilde{R}_{ij}(\underline{r}) = [f(r)-g(r)] \frac{r_i r_j}{r^2} + g(r)\, \delta_{ij} \quad , \quad i,j = u, v, w$$

where δ_{ij} is the Kronecker delta and $r_u \equiv r_x$, etc. Similarly, the three-dimensional spectrum tensor $E_{ij}(\underline{k})$ may be expressed as a fairly compact function in isotropic turbulence by

$$E_{ij}(\underline{k}) = \frac{E(k)}{16\pi^3 k^4} (k^2 \delta_{ij} - k_i k_j)$$

where

$$k = |\underline{k}| = \sqrt{k_x^2 + k_y^2 + k_z^2}$$

and $E(k)$ is a scalar function usually referred to as the 'energy spectrum function'. As for the $\phi_{ij}(n)$ spectra, isotropy requires that

$$\phi_{ij}(n) = 0 \quad , \quad i \neq j$$

and thus from Eq. (28),

$$\gamma_{ij} = 0, \quad i \neq j . \tag{33}$$

Also,

$$\phi_{vv}(n) = \phi_{ww}(n)$$

and Eq.(32) may be used to show that

$$\phi_{ww}(n) = \tfrac{1}{2} \phi_{uu}(n) - \frac{n}{2} \frac{d\phi_{uu}(n)}{dn} . \tag{34}$$

Because of Eqs. (30) and (31), all longitudinal integral scales are equal to each other in isotropic turbulence, as are lateral scales. That is,

$$L_u^x = L_v^y = L_w^z \equiv L_u \tag{35}$$

and

$$L_u^y = L_u^z = L_v^x = L_v^z = L_w^x = L_w^y \equiv L_v$$

and from Eq. (32), it can be shown that

$$L_u = 2 L_v . \tag{36}$$

Finally, the velocity component mean-square values are equal in isotropic turbulence, such that

$$\overline{u^2} = \overline{v^2} = \overline{w^2} = \sigma^2$$

and the Reynolds Stress tensor, for example, is now given by

$$R_{ij} = \begin{bmatrix} \sigma^2 & 0 & 0 \\ 0 & \sigma^2 & 0 \\ 0 & 0 & \sigma^2 \end{bmatrix} \qquad (37)$$

III. CHARACTERISTICS OF THE PLANETARY BOUNDARY LAYER

3.1 General Description

The atmosphere near the surface of the earth can conveniently be divided into three regions. These regions are the free atmosphere, the planetary boundary layer, and the surface boundary layer. In the free atmosphere, viscosity is neglected, and only inertial, Coriolis, and pressure gradient forces act on the air. The wind resulting from these forces is called the gradient wind, and is independent of the nature of the earth's surface below. It can easily be shown (Ref.3) that the gradient wind must flow along the isobars, and in the special case when the isobars are straight or so slightly curved that centripetal acceleration of the air is negligible, the gradient wind is called the 'geostrophic' wind and is given approximately by

$$\bar{U}_G = \frac{1}{\rho f} \frac{\partial p}{\partial \underline{n}}$$

where $\underline{n}$ is normal to the isobars and $f = 2\omega\sin\phi$, with ω the rotational velocity of the earth and ϕ the latitude.

The planetary boundary layer refers to the region between the earth's surface and the height at which the free atmosphere can be said to begin. This height is called the 'gradient height', z_G and is generally of the order of 1000-2000 feet, depending on surface conditions. The surface boundary layer is a sublayer of the planetary layer, extending from the ground up to about 200 ft. ($\pm$ 100 ft.) depending again on surface conditions. In the surface layer, Coriolis forces are assumed negligible, and wind characteristics are determined by surface conditions, thermal stability and height. Shear stress is assumed constant here, and indeed this actually defines the extent of the region. In the remainder of the planetary layer above the surface layer, Coriolis forces begin to have an effect on the wind, surface roughness effects decrease, and the shear stress decreases from its constant value in the surface layer.

In this review, it is the planetary layer that is being considered, and consequently the basic parameters of interest will be the surface conditions, thermal stability, and the height.

3.2 Atmospheric Stability

The hydrostatic stability of the atmosphere depends of course on the temperature gradients in it. The basic criterion is whether or not the decrease in temperature with height, called the lapse rate γ, is greater than the dry adiabatic lapse rate, Γ($\Gamma \approx 1^{\circ}C/100$ m. $\approx 5.5^{\circ}F/1000$ ft). During a 'lapse' period, when

$$\gamma \equiv -dT/dz > \Gamma$$

a volume of air displaced upward will experience a buoyant force upward and thus will continue to ascend. Thus the atmosphere in lapse periods is classified as 'hydrostatically unstable', or simply unstable. During so-called 'inversion' periods, when $\gamma < \Gamma$, the volume of air displaced upward will be at a lower temperature than its surroundings and will experience a restoring downward force, in which case the atmosphere is classified stable. If $\gamma \approx \Gamma$ or very slightly less, the atmosphere is classified neutral.

As for the effect of stability on turbulence in the atmosphere, one would obviously expect greater turbulence levels in hydrostatically unstable air since under these conditions, heat convection would be added to the 'mechanical' turbulence produced by the shear. A better understanding is obtained if one considers the driving force in moving vertically the volumes of air mentioned above. The energy required to displace the air, that is, to produce turbulence, is extracted from the mean flow by the Reynolds Stress. Whether the velocity fluctuations increase or decrease will depend on whether or not the rate of this energy supply is greater than the rate at which work must be done in the gravitational field in moving the fluid volumes in the vertical direction. The parameter expressing this criterion is the gradient Richardson Number, Ri, defined by

$$Ri \equiv \frac{g(\partial\theta/\partial z)}{\theta(\partial\bar{U}/\partial z)^2} . \tag{38}$$

Between zero and unity there is a 'critical' Richardson Number above which turbulent motion in the air will subside into laminar motion and below which it will remain turbulent. A definite value of this critical number is not available, and indeed it may depend on surface conditions. There is some indication (Ref's. 3 and 4), however, that it should be Ri $\sim$ 0.25, such that above this value of Ri turbulence ceases to exist.

Hydrostatic stability can easily be expressed in terms of Richardson Number. For an ideal gas, the potential temperature θ is related to the actual temperature T by

$$\frac{1}{\theta}\frac{\partial\theta}{\partial z} = \frac{1}{T}\left(\frac{\partial T}{\partial z} + \Gamma\right) .$$

Thus from Eq.(38),

$$Ri = \frac{g(\partial T/\partial z + \Gamma)}{T(\partial\bar{U}/\partial z)^2}$$

$$= \frac{g(\Gamma - \gamma)}{T(\partial\bar{U}/\partial z)^2} . \tag{39}$$

Therefore unstable air corresponds to $R_i < 0$ and stable air to $R_i > 0$.

Summarizing, then, the atmosphere may be characterized by the following Richardson number régimes::

$Ri < 0$	unstable air, with considerable convective turbulence in addition to the mechanical turbulence
$R_i \sim 0$	generally for $\|Ri\| <\sim 0.03$, the air is termed neutral or 'near-neutral' and the turbulence is purely mechanical
$0 < Ri <\sim 0.25$	stable air, with mechanical turbulence being damped by the thermal stratification
$R_i > \sim 0.25$	very stable air in which no turbulence can exist at all, at least in the vertical direction

The Richardson number is very important in the atmosphere since the Reynolds numbers are so large that they cease to be of importance, and Ri is the most relevant non-dimensional number.

3.3 Simplifying Assumptions

3.3.1 Stationarity

Spectral data measured by aircraft at different times in the planetary layer have shown that stationarity of the velocity signals can reasonably be assumed for periods up to 10-20 minutes, and sometimes longer. Thus reasonable record lengths can be obtained for the data without the stationarity assumption breaking down.

3.3.2 Homogeneity

It is generally assumed that the flow in the planetary layer is homogeneous in all horizontal planes, such that aircraft measurements obtained in any direction in these planes may be treated. Gunter et al (Ref.43) go so far as to conclude complete homogeneity of the turbulence based on measurements at 250 ft. and 750 ft. However, this conclusion seems somewhat optimistic, and indeed, some of the data presented refutes this conclusion since they find a definite increase in integral scale with height. Consequently only the concept of horizontal homogeneity is considered acceptable, and results show that in general this is a quite reasonable assumption, particularly over relatively homogeneous terrain.

3.3.3 Isotropy

In the free atmosphere, isotropy is a fairly reasonable assumption, but this proves less tenable with decreasing altitude. Lappe, Davidson and Notess (Ref.19) concluded from tower and aircraft measurements at $z \sim 300$ ft. in unstable air that Taylor's Hypothesis is roughly equally well satisfied regardless of what direction the aircraft flies relative to the wind. This would indicate that the turbulence under these conditions is more or less horizontally isotropic. Gunter et al (Ref.43) tested isotropy for hundreds of hours of aircraft data taken at $z = 250$ ft. and 750 ft. (i.e., generally above the surface layer) by comparing experimental ratios of vertical-to-lateral and longitudinal-to-lateral component spectra with the corresponding ratios obtained from the isotropic von Kármán spectral equations. Their conclusion is that for most stability cases and for all combinations of height and surface conditions, the turbulence is totally isotropic.

This conclusion is enhanced by γ_{uv}^2 and γ_{vw}^2 coherence measurements, which were always less than 0.15 for all frequencies, and would of course be zero for isotropic turbulence. It is to be noted, however, that the γ_{uw}^2 coherences, which one would expect to be larger than the other two in a shear flow, were not presented. Also, upon inspecting the presented data, it is seen that the conclusion of isotropy depends largely on the size of the difference between the theoretically isotropic case and the experimental data that is allowed for the data to be called isotropic. Within roughly 20% variation, the data is indeed seen to indicate isotropy, although the variation of scale with height still precludes true isotropy. It is evident from the data, however, that there is a distinct reduced frequency $k \approx 3 \times 10^{-3}$ cpf. above which there is a very significant decrease in the amount of departure of the data from the isotropic case. This suggests a 'local isotropy' region in which the turbulence is significantly closer to true isotropy than at lower frequencies.

The concept of local isotropy was first put forth by Kolmogoroff. It postulates that in the so-called inertial subrange region of the energy spectrum, the turbulence is isotropic. In this region turbulent energy is neither produced nor dissipated, but merely passed through from the large anisotropic eddies to smaller eddies by inertial forces. This energy is then dissipated by viscous forces at the same rate ϵ at which it is inertially passed through the subrange, maintaining an equilibrium state. Kolmogoroff showed that in this inertial subrange, the energy spectrum will be proportional to the -5/3 power of frequency, and the ratio of longitudinal-to-lateral or longitudinal-to-vertical spectra must be 3/4. The longitudinal component power spectrum in this region is of the form

$$\Phi_{uu}(k) = b\, \epsilon^{2/3}\, k^{-5/3}$$

where b is a constant, while the lateral and vertical component spectra are given by similar expressions but with b replaced by 4b/3. In the planetary layer, this notion of local isotropy seems quite reasonable, in that one would expect anisotropy for eddies large enough to be affected by the mean shear and thermal structure, while smaller eddies with shorter time scales should be able to redistribute their energy among the components more quickly. Thus one would expect that over a range of wavelengths small compared with some characteristic length, say the distance to the ground, z, or to the nearest stable layer, the turbulence should be isotropic.

Experimental results have in general tended to confirm the local isotropy concept, with some reservations. The spectra generally obey the -5/3 power law, with the constant b having a value of ~0.5 if k is in radians/m or ~0.065 if k,is in cycles/ft. However, there is some disagreement as to whether the 3/4 ratio of the spectra in the subrange actually exists. Elderkin (Ref.17) found for spectra at z = 10 ft. and 20 ft. that the longitudinal and vertical spectra are about the same in magnitude in the inertial range, and refers to some results by Stewart that found the same tendency. Also Berman (Ref.40) quotes several papers and states that the conclusion from these results is that all component spectra have the same magnitude in the subrange and not the Kolmogoroff ratios. On the other hand, however, Busch and Panofsky (Ref.41) studied considerable data for heights up to 300 ft. and concluded that in regions over which the spectra obey -5/3 power laws, the ratios of the components "show fair agreement" with the 3/4 ratios predicted by Kolmogoroff. In addition, Fichtl and McVehil (Ref.39) assumed the 3/4 ratio in obtaining model equations for the longitudinal and lateral components which ultimately fit measured data very well, thus indicating this ratio

to be valid for at least these components. Finally, the aircraft data obtained by Gunter et al obeyed the Kolmogoroff ratios quite well in the inertial subrange. In view of these discrepancies, no definite conclusion can be drawn as to whether the Kolmogoroff ratios are or are not obeyed.

There is far better agreement among investigators as to the validity of the -5/3 power law for the spectra. The data generally show that the spectra obey a -5/3 frequency dependence up to wavelengths much greater than can possibly be expected to lie in the Kolmogoroff inertial subrange, especially in the case of the longitudinal spectrum. However, it is not necessarily the case that this represents a simple extrapolation of this subrange (see Ref.41). As for the actual 'isotropic limit' above which local isotropy exists, considerable information is available. Lumley and Panofsky (Ref.4) give a detailed discussion of the limiting frequency, and quote a result from Priestley based on co-spectral measurements that local isotropy exists for $k \gtrsim 0.6/z$. Elderkin (Ref.17) concludes that while the -5/3 law is obeyed to frequencies as low as $k \sim 0.2/z$ in some cases, the co-spectra do not reduce to zero until $k \sim 3/z$, and true local isotropy is not attained for $k < \sim 4/z$. Lappe and Davidson (Ref.38) state that the Kolmogoroff range can exist, if at all, only for wavelengths less than 88 ft. based on measurements made at $z = 400$ ft., which suggests k must be greater than $\sim 4/z$. Finally, the value of k quoted above from the data of Gunter et al, above which isotropy improves ($k \approx 3 \times 10^{-3}$ cpf.), corresponds to an isotropic limit of $k \sim 1/z - 2/z$ for the heights measured, a value roughly in agreement with that suggested by Panofsky in Ref.63. Thus it appears that a reasonable value of reduced frequency above which local isotropy can be said to exist is $k \sim 3/z$.

To summarize, it can generally be said that turbulence in the planetary layer is not isotropic in the true sense. However, a region of local isotropy does exist for $k > \sim 3/z$, although the component spectra may or may not obey the Kolmogoroff ratios in this region. Horizontal isotropy, in which the turbulence is independent of rotations of the coordinate system about the vertical axis, is also a reasonable assumption.

3.3.4 Taylor's Hypothesis

Lin (Ref.55) has investigated the validity of applying Taylor's Hypothesis to the turbulence in shear flows and concludes that the requirement of $u' \ll \bar{U}$ should be valid for k such that

$$k \gg \frac{1}{\bar{U}} \frac{d\bar{U}}{dz} . \qquad (40)$$

If the logarithmic velocity law is assumed to hold (Eq.(42), Sec.3.4) then Eq. (40) becomes

$$k \gg \frac{1}{z \ln (z/z_o)} . \qquad (41)$$

Lappe and Davidson (Ref.38) compared aircraft and tower measurements at z = 300-400 ft. and found that the spectra so measured were the same for wavelengths at least as large as 600-900 ft. Since z_o for these tests was ~3.3 ft. (Ref.19), Eq. (41) suggests that in this case, $k \gg \sim 0.0005$ rpf. for Taylor's Hypothesis to be valid, or

$$\lambda = \frac{1}{k} \ll 2000 \text{ ft.}$$

Thus Lappe and Davidson's result roughly obeys Lin's requirement. In any case, it must be realized that Taylor's Hypothesis becomes decreasingly accurate for $\lambda > \sim 1000$ ft.

3.4 Mean Wind Characteristics

3.4.1 Velocity Profiles

In the surface boundary layer, the validity of the Prandtl logarithmic law for the mean velocity in a neutral atmosphere has been well-verified. The law can be easily obtained from Prandtl's Mixing Length theory (or von Kármán's similarity hypothesis) under the assumptions that

(i) viscous stress is negligible;

(ii) mixing length is proportional to height; that is, $\ell = Kz$;

(iii) shearing stress is constant and equal to the surface stress τ_o. That is,

$$\tau = -\rho\overline{uw} = \tau_o \equiv \bar{U}_\tau^2 \rho$$

where $\bar{U}_\tau$ is the friction velocity and is defined by the above relation.

If in addition $\bar{U} = 0$ at $z = z_o$ and it is assumed that $z_o \ll z$, the law can be written in the form

$$\frac{\bar{U}}{\bar{U}_\tau} = \frac{1}{K} \ln\left(\frac{z}{z_o}\right) \tag{42}$$

where K is the von Kármán constant (~0.4) and z_o is the so-called 'roughness length'.

The logarithmic law of Eq.(42) is valid strictly speaking only for neutral conditions. In non-neutral stabilities, a modification of this law is given (Ref.4 or 44) such that

$$\frac{\bar{U}}{\bar{U}_\tau} = \frac{1}{K}\left[\ln\left(\frac{z}{z_o}\right) - \psi\left(\frac{z}{L'}\right)\right] \tag{43}$$

where L' is a temperature dependent scaling length. The function ψ is a universal function of z/L' and since it can be shown that the Richardson Number is a unique function of z/L' (Ref.4), Eq.(43) can be used to obtain mean velocity in non-neutral stabilities.

The roughness length z_o usually turns out to be about 1/30 times the average dimension of a typical roughness particle. In practice, both z_o and $\bar{U}_\tau$ are determined from measurements of at least two values of $\bar{U}$ and z in the surface layer and solution of Eq. (43). An excellent description of the details of the procedure used to determine these quantities with the greatest possible accuracy is given in Ref. 44.

Above the surface layer, Coriolis forces increase, surface roughness effects decrease, and the logarithmic law begins to depart from the empirical data. However, treating the planetary layer as a whole, a power law velocity

profile of the form

$$\bar{U}/\bar{U}_1 = (z/z_1)^{\alpha} \tag{44}$$

is found to fit the data quite well in neutral conditions, where $\bar{U}_1$ is the velocity at some reference height z_1. Davenport (Ref's. 9 and 10) uses the gradient height as the reference height, such that

$$\bar{U}/\bar{U}_G = (z/z_G)^{\alpha}. \tag{45}$$

The parameters z_G and α depend on surface conditions, and Davenport (Ref.42) has surveyed published wind profiles at sites having a wide range of z_o values in order to determine the dependence of these parameters on z_o. The results of this survey are given in Fig. 1, and the shape of the profile given by Eq. (45) for three different terrain types is shown in Fig.2. The gradient height z_G must in general be obtained by measurement of $\bar{U}$ at several heights and an estimate of the gradient velocity $\bar{U}_G$. Thus there is some uncertainty in its exact value since $\bar{U}_G$ is usually obtained from isobaric charts whose accuracy depends on the spacing between the meteorological stations from which the pressure readings are obtained. However recent estimates of both z_G and α have shown good agreement with the values suggested by Fig. 1, including the results for various cities around the world given by Davenport in Ref. 10. It must be remembered, of course, that the power law can be of only limited usefulness in cities, since it cannot be expected to apply to the mean wind speed for heights considerably below typical obstructions. In cities these obstructions may be up to 700-800 ft. high, and the wind speed is very much a function of the detailed nature of the structures. Harris (Ref.58) states that it is not certain at the present whether, for the treatment of winds above a city, it is more correct to use a power law with large α as Davenport suggests, or to use a lower index combined with an upwards displacement of the $\bar{U} = 0$ reference plane to take account of the obstruction height. However, it would appear from the data that Davenport's approach is quite reasonable in those regions where any power law can be expected to apply.

In applying Eq. (45) to estimate gust loads on buildings, it is the extreme values of the mean wind that are of importance. Thus the values used for $\bar{U}_G$ is in general based on surface measurements of extreme wind speeds, and Davenport (Ref's. 9, 10 and 42) outlines in detail the procedure for estimating extreme values of $\bar{U}_G$ from local meteorological data.

As for the effect of stability on the shape of the power law profile, little data is available. In general, however, the exponent α tends to become smaller with decreasing stability. That is, in unstable air, the profile is generally 'fuller'.

3.4.2 Mean Wind Direction

It is not only the magnitude of the mean wind in the planetary layer which is important but also the direction, particularly in the consideration of the wind loading of structures. In the free atmosphere, the mean wind is the gradient wind, and it flows along the isobars. However, in the planetary layer, the presence of shear stresses in combination with the Coriolis forces causes a systematic deflection of the mean wind. This deflection is away from the isobars in the direction of decreasing pressure gradient, and is such that in the Northern Hemisphere the wind direction rotates clockwise with increasing height. Several theories have been postulated as to the exact variation with height of

the angle α between the mean wind and the isobars (i.e., the geostrophic direction), but they all require assumptions about the exchange of momentum due to turbulence at various heights. This exchange is represented by the eddy viscosity K_M where

$$K_M = \frac{-\overline{uw}}{\partial\bar{U}/\partial z} .$$

The simplest theory is due to Ekman and is outlined by Sutton in Ref.3. Ekman assumed K_M constant with height and as a result predicted that α should decrease from 45° at the surface to zero at the gradient height. This work has led to the change of wind direction with height being referred to as the 'Ekman Spiral'. Ekman's theory is somewhat of an oversimplification, however, and Sutton describes more sophisticated theories. One approach by Kohler assumes $K_M = K_1 z^m$ where m depends mainly on stability, and predicts that at the surface, α lies between 10° and 30°, decreasing of course to zero at z_G. Sutton's theory predicts values of α ranging from 31° in open country to 45° in city centres. In general, although little data is available over urban areas, other measurements have indicated values of α at the surface of the order of 20°, agreeing roughly with the theory. However, Harris in Ref.58 has suggested that very little of the decrease in α with height occurs in the first 600 ft. or so. His results in high winds (i.e., neutral stability) over flat terrain for z up to 600 ft. show no systematic deviation in wind direction, and he states that other results have tended to agree. Harris thus suggests that except for very tall structures or those with special features making them extremely sensitive to wind direction, it should be reasonable to ignore the change of wind direction with height in strong winds over all types of terrain.

3.5 Reynolds Stresses

3.5.1 Total Kinetic Energy of Turbulence

The parameters governing the magnitudes of the variances u', v', and w' of the velocity components, and thus the total kinetic energy of the turbulence, $\bar{e}$, are mean velocity, surface roughness, height, and stability. Similarity theory predicts that for neutral air, the total kinetic energy is roughly proportional to $\bar{U}_\tau^2$, indicating that this energy should thus be independent of height. Thus from Eq. (42) we get

$$\bar{e} \propto \bar{U}_\tau^2 = \frac{K\bar{U}^2}{\ln^2(z/z_o)} \qquad (46)$$

for the surface layer, and the data (viz. Ref.4) show that in general the variation of $\bar{e}$ with both velocity and height indicated by Eq. (46) is roughly correct. The effect of surface conditions, however, is not adequately represented by the roughness length z_o. This result is not surprising since z_o is a measure only of the small scale features of the surface and does not account for large irregularities such as hills and mountains. As for stability, a decrease tends generally to increase the total energy, due to the additional convective energy in unstable air. This effect is minimized over rough terrain, where most of the turbulence is of mechanical origin.

3.5.2 Vertical Component Variance

Similarity theory predicts that in neutral stability,

$$w' = A \bar{U}_T \tag{47}$$

where A is a constant independent of height, windspeed, and surface roughness. The data of various investigators (viz. Ref's. 17, 29, and 41) has shown this to be true at least through the surface layer, indicating that the effect of surface conditions on w' is adequately represented by $\bar{U}_T$, and thus by z_o (from Eq. (42)). That this is so for the w' component likely results from the fact that very large wavelength, low frequency components of w' are suppressed due to the presence of the ground, and thus the effect of large scale non-uniformities is reduced.

As for the value of the constant A in Eq. (47), there is considerable discrepancy in the data. Lumley and Panofsky (Ref.4) point out that values ranging from 0.7 to 1.3 have been obtained, and suggest that A ~ 1.0 is the best compromise. However, more recent data has leaned toward a value of ~ 1.3. Elderkin (Ref.17) obtained a value of 1.33 for z = 10-20 ft., while Busch and Panofsky (Ref.41) obtained 1.29 from an integration of their model spectrum, and state that this value is consistent with direct measurements made using sonic anemometers. Also, Panofsky and McCormack (Ref.29) found a value of ~ 1.3 for heights up to about 250 ft. and Panofsky in Ref.63 shows some results indicating that A = 1.3 over a considerable range of Richardson numbers. Thus it is concluded that A = 1.3 is the most appropriate value in view of the existing data.

The effect of atmospheric stability on w' is in general not too large. The magnitude of w' tends to increase somewhat with decreasing stability, as one would expect. In addition, w' increases slowly with height in unstable air, while in stable air it decreases with height. Thus stability effects on w' tend to be felt more at higher values of z, and are not too important near the ground.

3.5.3 Lateral Component Variance

In neutral air, at least, most of the existing data show that through the surface layer,

$$v' = B \bar{U}_T \tag{48}$$

where B is a constant. This suggests that v' does not vary with height in neutral air. One notable exception to this conclusion is the investigation by Fichtl and McVehil (Ref.39) whose tower data measured for heights up to ~ 500 ft. indicate that in neutral air, v' decreases slightly with height, being proportional to $z^{-.175}$ over this range. As for the dependence of v' on surface conditions, the roughness z_o is unfortunately inadequate to completely estimate the surface effect, as is the case for the total kinetic energy. Consequently, the constant B is a function of large scale roughness and thus varies from place to place, ranging from 1.3 to 2.6 (Ref.4).

Atmospheric stability has a quite large effect on v', increasing it by a large amount as stability decreases for the same wind speed. Lumley and Panofsky (Ref.4) show, however, that in either stable or unstable air, there is still very little vertical variation of v'. In this case, Fichtl and McVehil's results agree since they find that in unstable air, $v' \propto z^{-0.02}$, indicating a very weak dependence of v' on height.

An interesting consequence of the differential behaviour of v' and w' with height in stable air is pointed out by Lumley and Panofsky. Since w' decreases with height in stable air while v' does not, smoke emitted at z ~ 300 ft. in an inversion meanders horizontally, with little vertical spreading. In fact, this meandering results from the presence of low frequency components in the spectrum of v (see Sec. 3.6.2).

3.5.4 Longitudinal Component Variance

While the longitudinal fluctuating velocity component is the largest of the three, its properties generally tend to be intermediate between those of v and w. Stability affects it more than the w component but not so drastically as it affects the v component. Lumley and Panofsky (Ref.4) indicate that u' does not vary with height in any stability, although the fluctuations in stable air tend to shift from high frequency near the ground to lower frequency at larger heights. The independence of u' with height is confirmed by data quoted by Templin (Ref.30) for unstable air and heights up to 500 ft. and by the results of Fichtl and McVehil (Ref.39) who for similar conditions find that $u' \propto z^{-0.07}$. In neutral stability, however, Fichtl and McVehil find that $u' \propto z^{-0.315}$, rather than being constant with height.

In neutral air, Lumley and Panofsky suggest that

$$u' = C\,\bar{U}_\tau \,. \tag{49}$$

As with the lateral component, the roughness length z_o is again not adequate to completely represent large scale variations in the terrain, and while C is constant with height, it varies from place to place. Values quoted range from 2.1 to 2.9, with the value of 2.5 suggested as a reasonable engineering approximation.

3.5.5 Summary of Variances

The preceding discussion of the three component variances referred for the most part to the surface boundary layer. In this layer, if neutral stability is assumed and the suggested values of the constants A, B, and C are used, the ratios of the component variances are given by

$$u'/v'/w'/\bar{U}_\tau = 2.5/2.0/1.3/1 \,. \tag{50}$$

Also, since the logarithmic law of Eq.(.42) is valid under these conditions, the friction velocity is given by

$$\bar{U}_\tau = \frac{\bar{U}}{2.5 \ln (z/z_o)}$$

and thus from Eqs. (47), (48), and (49) the component intensities are given by

$$\frac{u'}{\bar{U}} = \frac{1}{\ln (z/z_o)} \,, \quad \frac{v'}{\bar{U}} = \frac{0.80}{\ln(z/z_o)} \,, \text{ and } \frac{w'}{\bar{U}} = \frac{0.52}{\ln(z/z_o)} \,. \tag{51}$$

These curves are shown in Fig.3 for z_o = 3 cm, a value characteristic of flat, open country. Also shown are some actual measurements quoted in Ref.30 for Sale, Australia which has similar surface conditions (z_o = 1 cm), and these

values are seen to agree well with the predicted values.

For the planetary layer above the surface layer, little information has been presented because there does not appear to be a great deal of information available. This may result from the fact that most towers used for measurement do not reach heights far above the surface layer, so aircraft data is the only major source. Some useful measurements have been obtained by Harris (Ref.65) for heights up to about 600 ft. in neutral stability, and these are shown in Fig.3. It is seen that these results agree quite well with Eq.(51) for $u'/\bar{U}$ in the surface layer and with the Sale data above it.

Considerable data on the component variances at z = 250 ft. and 750 ft. is to be found in Ref.43. Unfortunately, since velocity values are not available, direct comparison with the above data cannot be made. However, the data suggests that both these heights be considered above the surface layer, and if this is done some useful conclusions can be drawn about u', v', and w' above the surface layer. First, within reasonable limits, $u' \approx v' \approx w'$ at each height. Also, increased surface roughness results in larger component variances, although the effect is felt more at 250 ft. than at 750 ft., as expected. In addition, for both heights there is an increase in the variance with decreasing stability, and finally, the variances decrease from 250 ft. to 750 ft. for virtually all stabilities. When these conclusions are considered together with the above results, it would appear that in general, above the surface layer, the three velocity component variances tend to decrease with height toward the same value, as is the case in a typical wall boundary layer (viz. Ref.2 or 60). Thus curves similar to those found in a wall boundary layer have been shown in Fig.3. The particular value that the variances approach must of course be that in the free atmosphere, which is very small and which would in the ideal case of no velocity gradients be zero.

3.5.6 Other Reynolds Stresses

The component variances discussed above are, of course, simply the roots of the diagonal components of the Reynolds Stress tensor, Eq. (7). The remaining Reynolds Stresses are the $\overline{uv}$, $\overline{vw}$ and $\overline{uw}$ co-variances (the tensor is Hermitian), which would of course be zero if the turbulence were isotropic. Elderkin (Ref.17) obtained values of these stresses in various stabilities at z = 10 ft. and 20 ft. over flat terrain having z_o = 3 cm. His results in neutral air show that the $\overline{vw}$ stresses are quite small compared to $\overline{uw}$, while $\overline{uv}$ values are larger than $\overline{vw}$ but still considerably less than $\overline{uw}$. For the $\overline{uw}$ stress, there is really not sufficient data to make significant conclusions about the assumption of constant stress in the surface layer, although the values at the two measurement heights do not in general show any larger variation than that between different runs at the same height.

In the surface layer, the friction velocity is given by (see Sec. 3.4.1).

$$\bar{U}_\tau = \sqrt{-\overline{uw}} \quad .$$

Thus if the air is neutrally stable and the ratios of the component variances of Eq.(50) are assumed, then the correlation coefficient for the u and w components is given by

$$\frac{\overline{uw}}{u'\,w'} = \frac{-\bar{U}_\tau^2}{(2.5\bar{U}_\tau)(1.3\bar{U}_\tau)} = -0.31. \qquad (52)$$

Above the surface layer, this value must decrease, since the shear decreases and uw falls to zero. As for uv and vw above the surface layer, little data is available, although the coherence data of Gunter et al (Sec. 3.3.3 and 3.6.4) suggests that these stresses are quite small.

3.6 One-Dimensional Spectral Density Functions

In general, the one-dimensional turbulence component power spectral densities $\Phi_{ii}(k)$ consist of three distinct regions: a low frequency region in which energy is put into the turbulent motion from the mean flow; a middle frequency equilibrium region in which no energy production or dissipation is occurring, and only an inertial transfer of energy toward smaller eddies is taking place (i.e., the Kolmogoroff inertial subrange); and a high frequency region in which turbulent energy is converted to heat by viscous dissipation (viscous subrange). The frequency dependence of $\Phi_{ii}(k)$ in these three regions is roughly given by k^0, $k^{-5/3}$, and k^{-7}, respectively. As with the component variances, the power spectra in general are dependent on height, surface roughness, mean velocity, and thermal stability.

In addition to the above general regions of the power spectra, the existence of a 'buoyant subrange' has been suggested for atmospheric turbulence spectra in stable conditions. In this region, a 'buoyant length' depending on the stratification is the factor limiting the inertial subrange, rather than the distance to the ground. Lumley and Panofsky (Ref.4) discuss the buoyant subrange at some length, and Busch and Panofsky (Ref.41) show experimental data suggesting that it does exist, at least for the vertical spectra, with a frequency dependence of the order of k^{-3} as suggested by Lumley (Ref.56).

The behaviour of the power spectra in the inertial subrange has been discussed at some length in Section 3.3.3 with regard to both the relative magnitudes of the components and their frequency dependence, and consequently there is only minimal attention given to this region in the discussion that follows.

3.6.1 Vertical Component Spectrum

The vertical velocity power spectrum $\Phi_{ww}(k)$ has been quite extensively investigated and a considerable amount is known about it. In general, it is found that below a height of roughly 150 ft.-200 ft. the spectrum obeys dynamic similarity. That is, it can be expressed as

$$\frac{k\Phi_{ww}(k)}{\overline{w^2}} = F(f, Ri) \qquad (53)$$

where F is a universal function, and $f = kz$, such that when the spectrum is plotted in similarity coordinates $k\Phi_{ww}(k)/\overline{w^2}$ vs. kz for fixed stability, it is independent of height, mean velocity, and surface roughness. In addition, the shape of the spectrum at these heights does not vary a great deal with stability, except perhaps in the unstable case when distinct low frequency convective peaks are found (viz. Ref.17 for z = 40 ft., and also z = 270 ft.). The maximum value of the non-dimensional spectrum as given by Eq. (53) was found to be ~ 0.2 by Elderkin and slightly larger (.23 - .3) by Busch and Panofsky (Ref.41).

While stability does not in general have too great an effect on the shape of the spectrum at low altitudes, it does tend to shift the spectrum as a

whole. A decrease in stability moves it toward lower frequencies (larger wavelengths) while an increase shifts it to higher frequencies. This is a reasonable effect, in that in stable air, convective energy is minimized and one would thus expect a reduction in the low frequency energy components. Thus if $f_p^w = k_p^w \cdot z$ is the value of f at which the non-dimensional spectrum has its maximum value, the effect of stability is indicated by changes in value of f_p^w. Above 160 ft., Busch and Panofsky have noted that stability affects not only f_p^w, but also the spectrum shape, with energies being concentrated around higher frequencies in stable air.

For regions close to the ground, one would expect the energy at low wave numbers to be limited by the presence of the surface. This suggests that the scale of the vertical component should increase with height. This is indeed the case since, as indicated by the similarity of the spectrum, f_p^w does not change with height for fixed stability. Thus k_p^w is inversely proportional to height, and since it is also inversely proportional to scale (see Sec.3.7), the scale is linearly dependent on height. Above 160 ft., Busch and Panofsky have shown that f_p^w begins to increase with height, indicating the breakdown of dynamic similarity and a weakening dependence of scale on height. More will be said concerning the height dependence of scale in Sec. 3.7.

Many analytical expressions have been suggested in the past in order to represent the power spectrum of the vertical component. Bowne and Anderson (Ref.5) list several of these expressions, and in their Fig. 15 compare them for similar conditions. Lumley and Panofsky (Ref.4) also discuss some of these spectra in detail. One well-known model is the Dryden spectrum, which can be obtained for isotropic turbulence by assuming that the correlation function $\tilde{R}_{uu}(r_x)$ is given by

$$f(r) = f_u(r_x) \equiv \tilde{R}_{uu}(r_x) = e^{-r_x/L_u^x} . \qquad (54)$$

Then using Eq.(32), the correlation $\tilde{R}_{ww}(r_x)$ may be obtained as

$$g(r) = g_w(r_x) \equiv \tilde{R}_{ww}(r_x) = (1-r_x/2L_u^x)\, e^{-r_x/L_u^x}$$

and the $\Phi_{ww}(k_x)$ power spectrum is found by Fourier transforming this correlation. Assuming Taylor's Hypothesis, this spectrum is given in the frequency domain by

$$\Phi_{ww}(k) = 2\,\overline{w^2}\, L_u^x \left\{ \frac{1 + 3\,(2\pi L_u^x k)^2}{[1 + (2\pi L_u^x k)^2]^2} \right\} \qquad (55)$$

where L_u^x is the longitudinal integral scale and has been assumed to be twice the vertical component scale L_w^x. This model, like several others, indicates a frequency dependence of k^{-2} in the inertial subrange, and because the recent data consistently show a -5/3 power law, these models have fallen out of use. Of the other models, the von Kármán equation is likely the best, since it captures the features of scale length, total variance, and the -5/3 slope. Like the Dryden model, it was developed for isotropic turbulence, and $L_u^x = 2\,L_w^x$ is assumed. The equation is

$$\Phi_{ww}(k) = 2\,\overline{w^2}\,L_u^x \left\{ \frac{1 + 188.4\,(L_u^x k)^2}{[1 + 70.7(L_u^x k)^2]^{11/6}} \right\}. \qquad (56)$$

Another good model is that suggested by Busch and Panofsky (Ref.41) for z up to 160 ft., nondimensionally given by

$$\frac{k\,\Phi_{ww}(k)}{\overline{w^2}} = \frac{0.632\ f/f_p^w}{1 + 1.5(f/f_p^w)^{5/3}} \qquad (57)$$

assuming $w' = 1.3\ \bar{U}_r$. In this expression, f_p^w is a function of stability only, and Busch and Panofsky relate f_p^w and stability in their paper.

For heights above the surface layer, the results presented by Gunter et al (Ref.43) leave little doubt that the von Kármán model spectrum best fits the experimental data. For lower heights, Fig.4 shows that while the Busch-Panofsky model of Eq. (57) provides a somewhat better fit to the data than the von Kármán equation at low frequencies, both models tend to underestimate the energy in this region. Thus in the interest of simplicity and since the scale parameter in Eq. (56) can be used to indicate stability effects as is f_p in Eq. (57), it is suggested that the von Kármán model with an appropriate value of scale (see Sec. 3.7 and 4.6) adequately describes the vertical component spectrum throughout the planetary layer.

3.6.2 Lateral Component Spectrum

The power spectrum $\Phi_{vv}(k)$ of the lateral velocity component does not in general obey similarity theory, except for large wave numbers in some cases. Also, in neutral and unstable conditions, there is little dependence of the shape of the spectrum on height, although the location of the peak k_p^v does apparently depend on height as suggested by the results of Fichtl and McVehil (Ref. 39), who found that for z = 60 -500 ft. in neutral air, $k_p^v \propto z^{-0.42}$ and in unstable air, $k_p^v \propto z^{-0.28}$. There is, however, a very large variation in both the magnitude and shape of this spectrum with stability. In addition to a tendency for the spectrum to shift as a whole toward lower frequencies for unstable conditions, decreasing stability also greatly increases the low frequency portions of the spectrum while leaving the high frequency part relatively unaffected. Thus for fixed wind speed the effect of decreasing the stability is to superimpose long period variations on the shorter, mechanically produced eddies. Consequently, the low frequency part of the spectrum depends mainly on stability while the high frequency part depends on roughness and velocity.

In stable air, height variation of $\Phi_{vv}(k)$ becomes more significant. Lumley and Panofsky (Ref.4) show data which indicates that while the low frequency part of the spectrum remains roughly constant with height, the high frequency part decreases rapidly. The relative invariance of the low frequency part suggests also that the total variance $\overline{v^2}$ tends not to vary too much with height, as indicated in Sec. 3.5.3. Recalling that $\overline{w^2}$ decreases with height in stable air, and since $k\Phi_{ww}(k)/\overline{w^2}$ is invariant with height (dynamic similarity) it follows that $\Phi_{ww}(k)$ decreases with height for all frequencies. Thus at heights of the order of 200-300 ft. in stable air, the low frequency components of $\Phi_{vv}(k)$ are

large relative to those of $\Phi_{ww}(k)$, explaining why smoke plumes in these conditions meander laterially with little vertical spreading.

The lateral component spectrum is more difficult to represent analytically than that of the vertical component because of the lack of similarity. The usual practice is to use the same model as for the vertical spectrum, but with $\overline{w^2}$ replaced by $\overline{v^2}$ and L_w^x replaced by L_v^x. In the case of the von Kármán model, this theoretically makes no difference, since in isotropic turbulence, $L_u^x = 2\,L_v^x = 2\,L_w^x$ and $\overline{v^2} = \overline{w^2}$, and the equation is

$$\Phi_{vv}(k) = 2\,\overline{v^2}\,L_u^x \left\{ \frac{1 + 188.4\,(L_u^x\,k)^2}{[1 + 70.7(L_u^x\,k)^2]^{11/6}} \cdot \right\} . \qquad (58)$$

Another equation that has been found appropriate is a modification of the Busch-Panofsky relation of Eq.(57) which Fichtl and McVehil fitted to their data. This equation is given non-dimensionally by

$$\frac{k\,\Phi_{vv}(k)}{\beta_v \bar{U}_T^2} = \frac{C_v\, f/f_p^v}{[1 + 1.5(f/f_p^v)^{r_v}]^{\beta r_v/3}} \qquad (59)$$

where C_v and r_v depend on stability and f_p^v and β_v depend on height and stability.

Above the surface layer, the results of Gunter et al (Ref.43) show that the von Kármán equation provides the best fit to the data for a wide range of conditions. Consequently it is suggested that, as with the vertical component, the von Kármán equation be used to model the lateral component spectrum throughout the planetary layer, using appropriate values of scale (see Sec.3.7 and 4.6).

3.6.3 Longitudinal Component Spectrum

3.6.3.1 Total Velocity Spectrum

The complete power spectrum of the total velocity in the longitudinal direction extends to much lower frequencies than those of the other two velocity components. This is due to the long period variations of the 'mean' wind speed $\bar{U}$ resulting from macrometeorological fluctuations, and $\bar{U}$ is, of couse, non-zero only in the longitudinal direction. The best data available for the complete spectrum of horizontal windspeed is that obtained by van der Hoven (Ref.32) at Brookhaven, and shown in Fig. 5. This spectrum was formed by piecing together several separate portions which were obtained at different times at z ~ 330 ft. Also shown in Fig. 5 for comparison are the periods of some common occurrences as obtained from Ref. 30, in addition to a pair of conjectural peaks suggested by Davenport (Ref.9) and not measured by van der Hoven.

Generally, the part of the complete spectrum measured by van der Hoven displays two major peaks. One of these peaks has a period of ~ 100 hours, and is characteristic of the large scale movement of pressure systems. The other major peak has a period of 1-2 minutes and is characteristic of the gusts and winds resulting from the modifying influence of the ground. It is this part of the curve, the 'gust' spectrum, which is represented by the fluctuating component

u(t) and which corresponds to the lateral and vertical component spectra already discussed. It is of major interest since it contains the frequency components which most seriously affect structures and aircraft. In between the two peaks, there is a minor peak with a period of about twelve hours which corresponds to the lulls in windspeed generally occurring at sunrise and sunset.

Between the gust peak and the twelve hour peak, there is an obvious region of very low energy extending from a period of ~5 minutes to ~5 hours. This region is referred to as the 'spectral' or 'micrometeorological gap' and it apparently exists for all stability and terrain conditions. It results from a lack of any physical processes capable of generating fluctuations having these periods, and is generally assumed to exist for all cases. This assumption does not take into account the occurrence of intense local storms such as thunderstorms and tornadoes, but these are usually of such local extent that their probability of occurrence at a particular location is negligibly small.

The existence of the spectral gap is indeed fortunate in that it allows a very clear distinction to be made between gusts and macrometeorological fluctuations. By defining the mean wind velocity $\bar{U}$ as the average over some period within the gap, it is conveniently separated from the gust velocities. Also, since the gap begins at periods as short as 5 minutes, estimates of $\bar{U}$ can be obtained from very reasonable record lengths. Indeed the meteorological estimates of mean wind in various countries throughout the world are based on averages over periods ranging from 5 minutes to one hour, and the existence of the spectral gap ensures that these estimates will be virtually the same.

3.6.3.2 Gust Velocity Spectrum

The spectrum $\Phi_{uu}(k)$ of the longitudinal gust component in the surface layer is in a sense intermediate between that of the vertical and lateral velocity components. The low frequency portion is affected more by stability changes than the high frequency region, so the shape of the spectrum is stability dependent. However, the dependence is not nearly as strong as that of the lateral component, while the vertical component shape is virtually independent of stability. It is noted also that, as for the other velocity components, decreasing stability shifts the spectrum to lower frequencies.

Under all conditions, the longitudinal component spectrum contains considerable energy at low frequencies, such that in stable and neutral air, when this energy is less than in unstable air, it is still considerably larger than that of the other two component spectra. This is an indication that in neutral and stable air, the larger eddies are elongated in the wind direction (see also Sec. 3.7). Another distinct feature of the longitudinal component spectrum is that the -5/3 power law extends to considerably larger wavelengths than it does for the other two spectra. Lumley and Panofsky (Ref.4) suggest it is obeyed down to $k \sim 0.2/z$, the value also found by Elderkin (Ref.17) and by Panofsky and van der Hoven (Ref.35).

In general, as with $\Phi_{vv}(k)$, the spectrum does not obey dynamic similarity except, perhaps, at very large wave numbers. When plotted in similarity coordinates, the spectra show a great variety of shape and position for neutral air (viz. Ref.40). The maximum value of $k\,\Phi_{uu}(k)/u^{*2}$ also varies, since Busch and Panofsky (Ref.41) found a value of roughly 0.18, assuming $u' = 2.5\,\bar{U}_{\tau}$, and Berman (Ref.40) obtained ~ 0.27 using the same assumption, while Elderkin (Ref.17)

found a value of 0.12 and Fichtl and McVehil (Ref.39)found ~ 0.13. Finally, the location of the spectral peak f_p^u violates dynamic similarity, in that its value tends in general to increase with height at all locations. This result is found by virtually all investigators, and as the value of f_p^u determines the scale of the longitudinal component, its variation will be discussed further in Sec. 3.7.

As has been done for the vertical component spectrum, a number of analytical expressions have been suggested to represent the longitudinal spectrum $\Phi_{uu}(k)$. The Davenport spectrum (Ref's. 9 or 10) is used extensively in the building aerodynamics field, but it predicts that at low frequencies, $\Phi_{uu}(k) \propto k$. This is inconsistent with the notion that $\Phi_{uu}(k)$ approaches a constant value proportional to the integral scale at low frequencies, and this model thus departs from the data at low frequencies. A modification of Davenport's spectrum which removes this objection has been suggested by Harris (Ref's. 58 or 62) but this turns out to be identical to the von Kármán spectrum below. The isotropic Dryden spectrum corresponding to Eq. (55) for the vertical component is given by

$$\Phi_{uu}(k) = \frac{4\,\overline{u^2}\,L_u^x}{1 + (2\pi L_u^x k)^2} \tag{60}$$

but like its counterpart, it is rejected due to the -2 slope it predicts for large k. The von Kármán model is

$$\Phi_{uu}(k) = \frac{4\,\overline{u^2}\,L_u^x}{[1 + 70.7(L_u^x k)^2]^{5/6}} \tag{61}$$

and it of course does not suffer from this objection. This is also the case for the model spectrum suggested by Fichtl and McVehil (Ref.39), similar to that suggested for the lateral component, which fits the data they obtained for neutral and unstable conditions up to z ~ 500 ft. This equation is, non-dimensionally,

$$\frac{k\,\Phi_{uu}(k)}{\beta_u\,\bar{U}_\tau^2} = \frac{C_u\,f/f_p^u}{[1 + 1.5(f/f_p^u)^{r_u}]^{5\,r_u/3}} \tag{62}$$

where C_u and r_u depend on stability and β_u and f_p^u depend on height and stability. Finally, Berman (Ref.40) has presented graphs which can be used to obtain spectral values for any frequency as a function of height and for different stabilities, for heights up to z ~ 450 ft.

The results of Gunter et al (Ref.43) above the surface layer show that, as for the lateral and vertical component spectra, the von Kármán model provides an excellent fit to the data for various stabilities and surface conditions, if a suitable scale value is used in the model. The curves of Fig. 6 show that it also fits the data well in the surface layer, at least for larger heights. The discrepancy between the results of Elderkin at z = 10-20 ft. and the other two curves emphasizes the difficulty in modelling the spectra due to the lack of dynamic similarity.

Figure 6 also shows horizontal bars to indicate the range of natural

frequencies important to aircraft and structures. These bars have been adapted from those of Templin (Ref.30) and are plotted for a representative height of z = 200 ft. For the 'tall buildings and bridges' bar, a mean velocity of 50 fps. has been assumed for a typical frequency range of from 0.1 to 1 cps.

It is to be noted that none of the model spectra for the three velocity components takes account of the viscous subrange in which $\Phi_{ii}(k) \propto k^{-7}$. This is in general not a serious omission since this region is usually beyond the frequency range that affects the motions of aircraft or the oscillations of exposed structures. However, as Templin shows in Ref.30, if simulation of the planetary boundary layer is attempted on too small a scale, the viscous subrange may well be near the region of interest, resulting in significant errors if it is ignored. This point should thus be considered when the scale of an experiment is being determined.

3.6.4 Cross-Spectra

In general, cross-spectral data is available only for the different velocity components at a single point, but as for the power spectral densities, it is only these spectra that are of major interest. For the $\Phi_{uv}(k)$ and $\Phi_{vw}(k)$ spectra, Gunter et al have obtained measurements at z = 250 ft. and 750 ft. for various roughness and stability conditions and have presented the results in the form of the coherences $\gamma_{uv}^2(k)$ and $\gamma_{vw}^2(k)$. As pointed out in Sec. 3.3.3, these coherences are generally less than ~ 0.15, and tend to be smallest for $k > \sim 2/z$. Elderkin (Ref.17) has measured the co-spectral parts of the cross-spectra, $C_{uv}(k)$ and $C_{vw}(k)$ for heights up to 260 ft. in various stabilities. His results are given typically by Fig's. 7 and 8 and while these co-spectra are not in general significantly smaller than the $C_{uw}(k)$ co-spectra, the values tend to be centered about the zero axis in most stability cases. Also, these co-spectra do not become truly zero for k less than about 3/z, with the values becoming larger for lower values of k. As for the quadrature component spectra $Q_{uv}(k)$ and $Q_{vw}(k)$, these are generally assumed to be zero.

The $\Phi_{uw}(k)$ cross-spectrum differs considerably from the other two cross-spectra above. The quadrature component $Q_{uw}(k)$ is generally quite small, but its sign is useful for indicating what part of a moving eddy with transverse vorticity contributed to the reading. Thus, very qualitatively, the height of the centre of gravity of an eddy having a particular frequency k_o can be estimated by knowing the sign of $Q_{uw}(k_o)$ at a few values of the height (see Ref.4). As for the co-spectrum $C_{uw}(k)$, it is negative at low frequencies, with the absolute value decreasing toward zero for increasing frequency. Elderkin's data show that it reaches zero at about the same frequency as do the $C_{uv}(k)$ and $C_{vw}(k)$ co-spectra, and thus while the small eddies may have considerable energy, they do not contribute to the correlations between the velocity components. This result has been known for some time, and is consistent with the concept of local isotropy. Elderkin also finds that as for the power spectra, there is a slight shift of $C_{uw}(k)$ toward higher frequency with increased stability. In addition, Elderkin's plot of this co-spectrum in similarity coordinates shows that, like the vertical velocity power spectrum, it displays fairly reasonable dynamic similarity. Indeed the cross spectrum $\Phi_{uw}(k)$ should not vary too much with altitude through the surface layer over homogeneous terrain, since the area under it is $\overline{uw}$ which is assumed constant.

Analytical representation of the $\Phi_{uw}(k)$ cross spectrum has been discussed by Lumley and Panofsky (Ref.4) on the basis of the similarity of the co-spectrum $C_{uw}(k)$. They have suggested an expression for $C_{uw}(k)$, but unfortunately this does not fit the data at very low frequencies or in the inertial subrange. A useful model for $\Phi_{uw}(k)$ has been suggested, however, by Case et al (Ref. 53), in which $Q_{uw}(k)$ is assumed zero such that $\Phi_{uw}(k) = C_{uw}(k)$. They used data taken near the wall in a wind tunnel boundary layer and also in the surface boundary layer over the ocean to obtain the root-coherence functions defined from Eq. (28) by

$$\gamma_{uw}(k) = \frac{|\Phi_{uw}(k)|}{[\Phi_{uu}(k)\Phi_{ww}(k)]^{1/2}} . \tag{63}$$

It was found that the expression

$$\gamma_{uw}(k) = \frac{\gamma_o}{[1 + 0.395(L_u x_k)^2]^{1/2}} \tag{64}$$

provided a good representation of the experimental data. The quantity γ_o is a constant whose value is determined by the power spectra $\Phi_{uu}(k)$ and $\Phi_{ww}(k)$ and the value of the Reynolds Stress coefficient $\overline{uw}/u'w'$. That is, from Eq. (24),

$$R_{uw} \equiv \overline{uw} = \tfrac{1}{2}\int_{-\infty}^{\infty} \Phi_{uw}(k)\, dk$$

$$= \int_{o}^{\infty} \Phi_{uw}(k)\, dk$$

since if $Q_{uw}(k)$ is zero, $\Phi_{uw}(k) = C_{uw}(k) = C_{uw}(-k)$. Also, since $C_{uw}(k)$ is negative at all values of k until it reaches zero, we may write

$$\overline{uw} = -\int_{o}^{\infty} |\Phi_{uw}(k)|\, dk.$$

Thus from Eq.(63), we get

$$\overline{uw} = -\int_{o}^{\infty} \gamma_{uw}(k)[\Phi_{uu}(k)\Phi_{ww}(k)]^{1/2}\, dk$$

and using Eq. (64),

$$\overline{uw} = -\gamma_o \int_{o}^{\infty} \left[\frac{\Phi_{uu}(k)\,\Phi_{ww}(k)}{1 + 0.395(L_u x_k)^2}\right]^{1/2} dk. \tag{65}$$

Now recall from Eq. (52) that in the surface layer,

$$\overline{uw} = -0.31\, u'\, w' = -0.31 \sqrt{\overline{u^2}}\ \sqrt{\overline{w^2}}\ ,$$

such that when this is combined with Eq. (65), we get

$$\gamma_o = \frac{0.31}{\int_0^\infty \left[\frac{\Phi_{uu}(k)/\overline{u^2} \cdot \Phi_{ww}(k)/\overline{w^2}}{1 + 0.395(L_u{}^x k)^2} \right]^{1/2} dk} \quad . \tag{66}$$

Thus γ_o can be found for any choice of the $\Phi_{uu}(k)$ and $\Phi_{ww}(k)$ spectra, and the cross spectrum is obtained from Eq's. (63) and (64) as

$$\Phi_{uw}(k) = -\gamma_o \left[\frac{\Phi_{uu}(k)\Phi_{ww}(k)}{1 + 0.395(L_u{}^x k)^2} \right]^{1/2} . \tag{67}$$

Evaluation of γ_o as a function of z has been done using the von Kármán spectra (Sec.4.5 and Fig.12).

3.6.5 Cross-Correlation Spectrum

Consider as a special case of the general correlation tensor of Eq.(3) the tensor

$$R_{ij}(r_x, r_y) \equiv R_{ij}(r_x, r_y, 0, 0). \tag{68}$$

In order to obtain a tensor of true two-dimensional spectrum functions, one would Fourier transform this tensor twice, such that

$$\Phi_{ij}(k_x, k_y) = 4 \iint_{-\infty}^{\infty} R_{ij}(r_x, r_y)\, e^{-i2\pi(k_x r_x + k_y r_y)}\, dr_x dr_y. \tag{69}$$

Similarly, if the correlations $R_{ij}(r_x)$ are Fourier transformed once, one gets a tensor of true one-dimensional spectrum functions

$$\Phi_{ij}(k_x) = 2 \int_{-\infty}^{\infty} R_{ij}(r_x)\, e^{-i2\pi k_x r_x}\, dr_x$$

as in Eq. (20a). However, suppose now that the two-dimensional correlation functions $R_{ij}(r_x, r_y)$ are transformed only once, with respect to r_x. In this case, the results are not true spectrum functions in the sense defined above, but neither are they correlation functions. The result of such a transformation is

$$\Psi_{ij}(k_x, r_y) = 2 \int_{-\infty}^{\infty} R_{ij}(r_x, r_y)\, e^{-i2\pi k_x r_x}\, dr_x. \tag{70}$$

Assuming Taylor's Hypothesis, k_x may be replaced by $k = n/\bar{U}$, and since $r_x = \bar{U}\tau$,

$$\Psi_{ij}(k, r_y) = 2\bar{U}\int_{-\infty}^{\infty} R_{ij}(r_y,\tau)\, e^{-i2\pi n\tau}\, d\tau \qquad (71)$$

for homogeneous turbulence. Indeed, if the turbulence is not homogeneous in the y-direction, this quantity is a function of the two points y_1 and y_2 which are separated by r_y rather than of only r_y. That is,

$$\Psi_{ij}(k, y_1, y_2) = 2\bar{U}\int_{-\infty}^{\infty} R_{ij}(y_1, y_2,\tau)\, e^{-i2\pi n\tau}\, d\tau\ .$$

This quantity can also be expressed in terms of a coherence function, defined by

$$\gamma_{ij}^{2}(k, y_1, y_2) \equiv \frac{|\Psi_{ij}(k, y_1, y_2)|^2}{\Phi_{ii}(k, y_1)\Phi_{jj}(k,y_2)} \qquad (72)$$

where $\Phi_{ii}(k,y_1)$ refers simply to the power spectrum $\Phi_{ii}(k)$ of the i-component obtained at y_1, and similarly for $\Phi_{jj}(k, y_2)$. Physically, $\Psi_{ij}(k, y_1, y_2)$ may be interpreted as the zero-time-delay cross-correlation (or mean product) of the parts of the two velocity components i and j contained in their respective spectra at the frequency k, and this has led Davenport (Refs.9 and 10) to use the term 'narrow-band cross-correlation', of which $\gamma_{ij}(k, y_1, y_2)$ as defined here is the magnitude. It may also be interpreted as the frequency distribution of the spatial cross-correlation of the i- and j-components, leading to the term 'cross-correlation spectrum' also used by Davenport. Finally, it is pointed out that since $\Psi_{ij}(k, y_1, y_2)$ is a form of cross-spectrum, it may be expressed as the sum of real and imaginary parts. That is,

$$\Psi_{ij}(k, y_1, y_2) \equiv C_{ij}(k, y_1, y_2) + i\, Q_{ij}(k, y_1, y_2)$$

and thus Eq. (72) becomes

$$\gamma_{ij}^{2}(k, y_1, y_2) = \frac{C_{ij}^{2}(k, y_1, y_2) + Q_{ij}^{2}(k, y_1, y_2)}{\Phi_{ii}(k, y_1)\,\Phi_{jj}(k, y_2)}\ .$$

In the case of homogeneous turbulence, $Q_{ij} \equiv 0$ and the y_1 and y_2 dependence is replaced by r_y such that

$$\gamma_{ij}^{2}(k,r_y) = \frac{C_{ij}^{2}(k, r_y)}{\Phi_{ii}(k)\Phi_{jj}(k)}\ . \qquad (73)$$

Davenport measured the quantity $\gamma_{uu}(k, r_y)$ as defined above for the longitudinal velocity components at two points separated laterally across a strong turbulent flow in a wind tunnel (see Ref's. 9 or 22). His results showed that for various values of r_y, the data collapsed on a curve given by

$$\gamma_{uu}(k, r_y) = e^{-ckr_y} \tag{74}$$

where $c \approx 8$. For the turbulence in the atmosphere, measurements have shown that for separations in the vertical direction, cross correlations of the longitudinal component indicate the existence of a similar relationship. That is, if the separation in the y-direction as above is replaced by separation in the z-direction and the coherence is defined by

$$\gamma_{ij}^2(k, r_z) = \frac{C_{ij}^2(k, r_z)}{\Phi_{ii}(k)\Phi_{jj}(k)} \tag{75}$$

then measurements at various vertical spacings have shown that

$$\begin{aligned}\gamma_{uu}(k, r_z) &= e^{-c_z k r_z} \\ &= e^{-c_z n r_z/\bar{U}} \\ &\equiv e^{-c_{10} n r_z/\bar{U}_{10}}\end{aligned} \tag{76}$$

where the coefficients c_{10} and c_z are defined depending on whether the velocity $\bar{U}$ at height z or $\bar{U}_{10}$ at z = 10 m. is used. Generally, the value $\bar{U}_{10}$ is preferable here, since the increase of $\bar{U}$ with height means that $\bar{U}$ is different at z_1 and z_2 and thus the question arises as to which value of $\bar{U}$ to use. Davenport in Ref. 10 quotes values of c_{10} ranging from 5 to 10 for heights from 300 to 830 ft. over various types of terrain. The coefficient appears to be independent of height, but seems to be generally smaller for rough surface conditions such as urban areas than for smooth surfaces.

Surry (Ref.12) investigated grid turbulence in a wind tunnel and found that a modified version of the Davenport relation of Eq, (74) better fits his data for $\gamma_{uu}(k, r_y)$ than the original expression. This modified empirical relation is

$$\gamma_{uu}(k, r_y) = e^{-(ckr_y)^a} \tag{77}$$

where $c \approx 6.4$ and $a \approx 1.4$. In addition, Surry points out that a curve of this form with a = 1.4 and c = 8 provides a better fit to Davenport's own data than Eq. (74). Finally, Harris (Ref.58) has shown that the data is better represented by a more complex analytical expression based on homogeneous isotropic theory. It can be shown for the von Kármán model that

$$\gamma_{uu}(n, r_y) = \frac{2}{\Gamma(5/6)}\left\{\left(\frac{\eta}{2}\right)^{5/6} K_{5/6}(\eta) - \left(\frac{\eta}{2}\right)^{11/6} K_{1/6}(\eta)\right\} \tag{78}$$

where $\eta = 2\pi r_y \bar{U}_{10} \sqrt{2 + \bar{n}^2} / L\bar{U}$ and $\bar{n} = nL/\bar{U}_{10}$. The parameter L is a length scale and $K_{5/6}$ and $K_{1/6}$ are modified Bessel functions of the second kind. If $\bar{n}^2 >> 2$, which is the case for most of the frequency range, the above expression for η becomes

$$\eta \approx 2\pi n r_y / \bar{U} = 2\pi k r_y$$

and direct comparison of Eq. (78) with the above empirical relations becomes quite simple. This comparison is shown in Fig. 9, along with experimental results measured in wind tunnel grid turbulence by Bearman and quoted by Harris in Ref. 58. It is seen that the theoretical expression is superior since it accounts for the negative portions of the curve, while the empirical curves do not. Indeed, neither Surry's nor Davenport's experimental data showed negative results, presumably because they found results only for η up to ~ 2.2.

As for atmospheric data, Harris compares data measured at points separated vertically above the surface with the corresponding theoretical expression

$$\gamma_{uu}(k, r_z) = \frac{2}{\Gamma(5/6)} \left\{ \left(\frac{\eta}{2}\right)^{5/6} K_{5/6}(\eta) - \left(\frac{\eta}{2}\right)^{11/6} K_{1/6}(\eta) \right\}$$

where $\eta \approx 2\pi k r_z$. His results show very good agreement for heights above the surface layer, but deterioration of this agreement within the surface layer. This result is not at all surprising, since it is an indication of the closer adherence of atmospheric turbulence to isotropic relations above the surface layer than in it, and this feature is indicated by virtually all the other turbulence data.

3.7 Integral Scales of Turbulence

Integral scales of turbulence have been defined in Sec. 2.2 and of the nine scales defined by Eqs.(12), the scales L_u^x, L_v^x and L_w^x of Eq. (12(a)) are of the most interest. In order to obtain estimates of these scales from experimental data, three basic methods can be used. The first of these is what might be called the direct method, since it involves obtaining the actual correlation curve in the scale definition and integrating to obtain the area under it. In the case of the above scales, the single point time correlation curve is generally measured and Taylor's Hypothesis assumed to convert the time scales so obtained to length scales. Thus, for example, from Eq. (16)

$$L_u^x = \bar{U} \int_0^\infty \tilde{R}_{uu}(\tau) d\tau = \frac{\bar{U}}{\overline{u^2}} \int_0^\infty R_{uu}(\tau)\, d\tau.$$

The difficulty that often occurs with this approach is that at the low frequency (large τ or spatial separation) end, the correlation does not approach zero asymptotically. Instead, due to the existence of very slow variations, the correlation obtained from a finite recording period has undulations about the zero axis at the low frequency end (viz.Ref's. 24 and 48). One attempt at avoiding this problem is the use of the second method for obtaining scales. In this method, one uses for the scale the value of the space (or time) separation at which the normalized correlation curve has dropped to a value of 1/e. Thus assuming the correlation is a true exponential, such that, for example,

$$R_{uu}(r_x) = e^{-r_x/L_u^x}$$

as in Eq. (54), then the above value of r_x is the true scale L_u^x. As one would expect, however, this is usually not the case, and some form of correction to this value is generally required. This correction usually requires the application of the first method at least a few times.

The third method for obtaining integral scales is from the one-dimensional power spectra. In all the model spectra, there is a free scale parameter which locates the curve on the frequency axis, and for the von Kármán or Dryden models, this parameter is the true integral scale L_u^x. For any particular model, this scale parameter can be related to the value k_p^i at which the non-dimensionalized spectrum has its maximum value. For example, from the von Kármán model for the longitudinal component spectrum, Eq. (61), we get

$$L_u^x = 0.146/k_p^u \tag{79}$$

while the Dryden model of Eq. (60) gives

$$L_u^x = 1/2\pi k_p^u = 0.159/k_p^u. \tag{80}$$

For the vertical component models, Eq. (56) yields

$$L_u^x = 0.212/k_p^w \tag{81}$$

and from Eq. (55)

$$L_u^x = 0.234/k_p^w. \tag{82}$$

The lateral component models will of course give the same expressions as Eq's. (81) and (82) with k_p^w replaced by k_p^v. Suppose now that either the von Kármán or the Dryden model is assumed to fit the experimental spectral data for a particular component. The scale can thus be simply obtained from the location k_p^i of the peak of the experimental curve by using the appropriate expression above. This method for obtaining scale estimates is used quite commonly, but it has two major drawbacks. In the first place, the peak of the experimental data is not always clearly defined, particularly for the longitudinal and lateral components, and it can therefore be difficult to obtain a good estimate of k_p^i. In addition, the peak is generally located near the low frequency end of the spectrum, where the data is not as reliable as it is at larger frequencies, and further errors may be introduced.

In obtaining scale values by the third method outlined above, considerable care must be exercised in interpreting exactly what has been obtained. As previously stated, both the von Kármán and the Dryden spectral models are for isotropic turbulence, and the vertical and lateral component models are written in terms of the longitudinal component scale L_u^x on the assumption that the isotropic relation $L_u^x = 2L_v^x = 2L_w^x$ is valid. However, if the turbulence is not isotropic, the isotropic models may still fit the experimental data quite well, but the above scale relation is not valid. In particular, this is the case in the lower atmosphere. Thus if one applies Eq. (81) or (82) to experimental

data for the vertical velocity component, it is in fact not L_u^x that has been obtained, but rather 2 L_w^x, and from this data one can obtain information only about the vertical component, not the longitudinal. This point explains why Taylor (Ref.51), for example, concludes that L_u^x is proportional to height z from the surface up to z = 1000 ft. when most results indicate a much weaker variation with height. Taylor's results are based on vertical component data taken from Saunders(Ref.20) and Panofsky and McCormack (Ref.29) and fitted with the von Kármán vertical component model. The data shows that k_p^w is proportional to height, such that while Eq. (81) indicates L_u^x should thus be proportional to height, it is in fact L_w^x that is proportional to height. No conclusions can be made about L_u^x except perhaps at larger heights where $L_u^x = 2L_w^x$ is a more reasonable approximation. Probably the best way to avoid confusion here when using the von Kármán or Dryden models is to replace L_u^x by $2L_v^x$ in the lateral component equation and by $2L_w^x$ in the vertical component equation. Thus for the von Kármán model, Eq's. (79) and (81) become

$$L_u^x = 0.146/k_p^u, \quad L_w^x = 0.106/k_p^w \tag{83}$$

and for the Dryden model, Eq's. (80) and (82) become

$$L_u^x = 0.159/k_p^u, \quad L_w^x = 0.117/k_p^w. \tag{84}$$

In the literature, the bulk of the data available is for the scales L_u^x and L_w^x. As one might expect, these scales are functions of height, thermal stability, and surface conditions since physically they represent the size of the predominant eddies in the turbulence. As with the longitudinal and lateral component variances, the effect of surface conditions is not adequately expressed by roughness length, since large scale non-uniformities such as hills and mountains have a significant influence on the scales. For example, the results of Berman (Ref.40) show little effect of roughness length on scale for uniform terrain while Lappe (Ref.28) indicates a distinct increase in scale with increasing surface non-uniformity. Lappe also shows that the effect of the surface is felt most strongly at lower heights, and that as height increases toward 1000 ft., terrain type becomes less important. This tendency was also found by Gunter et al (Ref.43) whose results show that increasing surface non-uniformity increases scale at z = 250 ft. but has little effect at 750 ft. Conversely, an increase of scales with decreasing stability was found by Gunter et al to be quite noticeable at z = 750 ft. but not at 250 ft. To summarize, then, it may be concluded that increasing surface non-uniformity tends in general to increase integral scales, but more so at small heights than at large; decreasing thermal stability tends to increase scale, but more so at large heights than at small. Also, roughness length has little effect on scales, while increasing large scale non-uniformities of the surface tends to increase them.

As for the effect of height on scale, it is generally agreed that all of L_u^x, L_v^x and L_w^x increase with height, although not necessarily in the same manner. The variation of the scale L_w^x of the vertical component is the one which is most consistently agreed upon. Figure 10 shows the results of most of the investigations of recent years, for neutral air over flat terrain unless otherwise noted. In all cases, the scales were obtained by the spectral fit method, and in the few cases when only the spectra were given, Eq. (83) was used

to determine L_w^x. It is noted also that for the data of Ref's. 20, 21 and 28, the published values for L_u^x were divided by 2 and used as L_w^x since these values were determined from vertical component data. It is evident that the scale L_w^x is in fact proportional to height as suggested previously, and a value of 0.40 for the constant of proportionality places the curve in the centre of the data within a reasonable amount of scatter. Thus it is suggested that the relation

$$L_w^x = 0.4\ z. \tag{85}$$

gives a reasonable estimate of this scale for heights up to 1000 ft. in neutral air over relatively flat terrain. It is also pointed out that if one considers only the region outside the surface layer in Fig. 10 (i.e., z = 200 or 300 ft. to z = 1000 ft.), the variation of L_w^x with height appears to weaken somewhat, as suggested by Busch and Panofsky (Ref. 41). The additional line shown in this region is given roughly by

$$L_w^x = 2.1\ z^{0.73} \tag{86}$$

and this may fit the data slightly better in this region than the $L_u^x = 0.4\ z$ relation.

The results available to date for the scale L_u^x at various heights in neutral air are shown in Fig. 11. Here again, most of the data were obtained by fitting spectral models to experimental data for the longitudinal component. It is obvious that there is considerably greater scatter in this data than in those for L_w^x. However, some definite conclusions can be drawn. First, it can be seen that there is a distinct increase in L_u^x with height over the entire range 0-1000 ft. Also, this increase with height is weaker than that for L_w^x, with Berman (Ref.40) suggesting $L_u^x \propto z^{0.25}$ and Webb concluding $L_u^x \propto z^{0.5}$. Thirdly, the data for the surface layer is considerably more conclusive than that for the remainder of the planetary layer. In the 0-200 ft. range, most of the data falls within the shaded band shown. The centre of this band is given by the line

$$L_u^x = 22.7\ z^{0.47} \tag{87}$$

and the extremities of the band are roughly 50-60% away from this line. Since this relation suggests more accuracy than is reasonable considering the scatter, the relation

$$L_u^x = 20\ \sqrt{z} \tag{88}$$

is also shown in Fig. 11, and it is seen to reasonably indicate the location of the band. Thus it is suggested that Eq. (88) be used to estimate L_u^x in the surface layer under these conditions, realizing that variations of the size shown are unavoidable due to the complexity of the atmosphere. Above 200 ft., Fig. 11 shows that Eq. (88) can also be used with a scatter in the data similar to that below 200 ft. However, it is to be noted that over the 200-1000 ft. range, a stronger or weaker variation could be the case, as the data are not too conclusive. In particular, the line $L_u^x = 0.8\ z$ is seen to fall within the scatter band, as is the line

$$L_u^x = 4.2\ z^{0.73}. \tag{89}$$

Both these lines represent the isotropic relation $L_u^x = 2L_w^x$ based on the

relations of Eq's. (85) and (86) for L_w^x in the 200-1000 ft. range. However, the line $L_u^x = 0.8\,z$ is seen to be completely unacceptable below z = 200 ft. Thus, here again, as from other observations, it is seen that if any form of isotropy exists in the lower atmosphere, it must certainly be outside the surface layer.

In Fig. 11, the fact that L_u^x increases with height is indicated by most of the data shown, including that of Davenport (Ref.37). This is contrary to the conclusion of Elderkin (Ref.17) and Fichtl and McVehil (Ref.39) who state that Davenport's data showed the peak of the longitudinal spectrum, and thus the scale L_u^x, to be invariant with height. However, the invariance of this data with height results only from the fact that the variable $n/\bar{U}_{10}$ was used as the abcissa, where $\bar{U}_{10}$ is the mean velocity at z = 10 m. Indeed, as Davenport himself points out in Ref.10, if $n/\bar{U}$ were used as the independent variable, where $\bar{U}$ is the mean velocity at height z, then the location of the peak, which would now be k_u as previously defined, would indeed show a variation with height. Thus the 'scale' L used by Davenport in Ref.10 (and which was equal to 1200 m. in Ref. 37) and also by Harris (Ref's. 58 and 62) is constant with height, but only because it was defined using $n/\bar{U}_{10}$. By comparing Harris' spectral model with that of von Kármán, this scale may be found in terms of the true integral scale as

$$L = \left(11.9\ \frac{\bar{U}_{10}}{\bar{U}}\right) L_u^x$$

and it is thus easily seen that since L is constant,

$$L_u^x \propto \bar{U}/\bar{U}_{10} \propto z^{\alpha}$$

using Eq. (44). Thus Davenport's results do not indicate constant longitudinal scale but rather that this scale increases with height in the same way as the mean velocity does.

Very little data is available for the scale L_v^x, and few definite conclusions can be drawn. Gunter et al (Ref.43) found that overall stabilities and terrain types, the average value of L_v^x was 180 ft. at z = 250 ft. and 230 ft. at z = 750 ft., these values being roughly equivalent to those found for L_w^x and half the values found for L_u^x. The spectra obtained by Fichtl and McVehil (Ref.39) were used to find that in neutral air,

$$L_v^x = 35.2\ z^{0.42}$$

for z ~60-500 ft., indicating a variation with height similar to that for L_u^x but yielding values that are roughly the same in magnitude as L_u^x rather than L_w^x. Elderkin's data for z = 10-20 ft. yields $L_v^x \approx z$, such that L_v^x is larger than the values of L_w^x obtained from his data but smaller than the L_u^x values so obtained. Thus about all that can be said about L_v^x is that it increases with height, and above the surface layer it is probably roughly the same as L_w^x.

As for the remaining scales defined by Eqs.(12), little information is available. Panofsky (Ref.24) gives some information based on correlation curves measured over smooth terrain (z_o = 1 cm) at z = 6.5 m. From so-called 'semi-scales'

obtained from these correlations, he found that in stable air, $L_u^x \sim 8\, L_u^y$, a result which was also found by Grant (Ref.25) in a wind tunnel boundary layer. Thus the eddies are elongated in the mean wind direction in stable air, and also presumably in neutral air. The lateral component scale was also found to be elongated in the mean wind direction in stable air, with $L_v^x \sim 3\, L_v^y$, and also $L_v^y \sim L_u^y$. In unstable air, however, Panofsky's results show an entirely different situation, in that L_u^x was found to be increased by a factor of about six over the stable air value, and all scales were roughly the same size, or $L_u^x \sim L_u^y \sim L_v^x \sim L_v^y$. Finally, Panofsky also found L_w^x and L_w^y much smaller than the other scales at this height for both stable and unstable air, a result not surprising considering the nearness of the surface. Thus the anistropy of the turbulence very near the surface is emphasized by these results, in addition to the strong effect of stability. Panofsky sums up his findings by stating that on a clear day (i.e., unstable air) the scales L_u^x, L_u^y, L_v^x, and L_v^y are all large and of the same order of magnitude, while at night (stable air) the scales are much smaller and that of the u-component is much smaller across the wind than along it. For a further qualitative description of the eddy structure in the atmosphere, the reader is referred to Ref. 4, page 210.

IV. MATHEMATICAL MODEL OF THE PLANETARY BOUNDARY LAYER

As a summary to the preceding description of flow characteristics in the planetary layer, a mathematical model is suggested, based on certain simplifying assumptions. This model is intended to be a compromise between precision and simplicity, and the validity of any part of it can be determined by referring to the appropriate section of the preceding discussion.

4.1 Assumptions

(1) The mean wind velocity is assumed to be strong enough such that the atmosphere may be considered neutrally stable.

(2) Taylor's Hypothesis, or the assumption of frozen flow, is assumed to be valid over the entire gust spectrum range of interest ($\lambda = \bar{U}/n \sim 50$-$7000$ ft).

(3) The gross features of the terrain are assumed to be relatively uniform, such that roughness length z_o represents the surface effects adequately.

(4) The flow is assumed stationary for periods at least as long as the record length used to obtain mean velocity values.

(5) The flow is assumed to be homogeneous in any horizontal plane.

4.2 Mean Velocity Profile

The mean velocity through the entire planetary layer ($z = 0$ to $\sim$ 2000 ft,) is given by

$$\bar{U}/\bar{U}_G = (z/z_G)^{\alpha}$$

where z_G and α are given in terms of surface roughness by Fig. 1 and the gradient wind $\bar{U}_G$ is determined from local meteorological data. For the surface layer alone ($z = 0$ to $\sim$200 ft.) the mean velocity is given by

$$\bar{U}/\bar{U}_\tau = 2.5 \ln (z/z_o)$$

where $\bar{U}_\tau$ is the friction velocity.

4.3 Reynolds Stresses

The ratios of the velocity component variances in the surface layer are given by

$$u'/v'/w'/\bar{U}_\tau = 2.5/2.0/1.3/1$$

and the turbulence intensities are

$$\frac{u'}{\bar{U}} = \frac{1}{\ln(z/z_o)}, \quad \frac{v'}{\bar{U}} = \frac{0.80}{\ln(z/z_o)}, \text{ and } \frac{w'}{\bar{U}} = \frac{0.52}{\ln(z/z_o)}.$$

Above the surface layer, the intensities all tend toward the same value, this value being determined by the turbulence intensity in the free atmosphere which is assumed to be zero.

The Reynolds Stresses $\overline{uv}$ and $\overline{vw}$ are assumed to be zero throughout the planetary layer. In the surface layer, the $\overline{uw}$ Reynolds Stress is determined by the variance ratios specified above, such that (Eq.52)

$$\overline{uw} / u'w' = -0.31.$$

Above the surface layer, $\overline{uw}$ decreases in magnitude toward zero.

4.4 Power Spectra

The von Kármán equations are suggested as the model for the velocity component power spectra. The appropriate (anistropic) values of integral scale and variance must be used, however, as specified. Thus the power spectra are given by

$$\Phi_{uu}(k) = \overline{u^2} \cdot \frac{4 L_u^x}{[1 + 70.7(L_u^x k)^2]^{5/6}} \tag{90}$$

$$\Phi_{vv}(k) = \overline{v^2} \cdot 4 L_v^x \left\{ \frac{1 + 188.4(2L_v^x k)^2}{[1 + 70.7(2L_v^x k)^2]^{11/6}} \right\} \tag{91}$$

$$\Phi_{ww}(k) = \overline{w^2} \cdot 4 L_w^x \left\{ \frac{1 + 188.4(2L_w^x k)^2}{[1 + 70.7(2L_w^x k)^2]^{11/6}} \right\} \tag{92}$$

4.5 Cross-Spectra

The cross-spectra $\Phi_{uv}(k)$ and $\Phi_{vw}(k)$ are assumed to be zero in this model, along with the quad-spectrum $Q_{uw}(k)$. The cross-spectrum $\Phi_{uw}(k)$ is thus equal to $C_{uw}(k)$ and is given in the surface layer by

$$\Phi_{uw}(k) = -\gamma_o \left[\frac{\Phi_{uu}(k)\, \Phi_{ww}(k)}{1 + 0.395(L_u^x k)^2} \right]^{1/2} \tag{93}$$

or in non-dimensional terms,

$$\gamma_{uw}(k) = \frac{\gamma_o}{[1 + 0.395(L_u^x k)^2]^{1/2}} . \tag{94}$$

The value of γ_o can be determined from Eq. (66) using the power spectra of Eqs. (90) and (92) and the scale values given in the following section. The variation of γ_o with height is determined completely by the ratio L_w^x/L_u^x, and this variation is shown in Fig.12 for L_w^x/L_u^x as found from Eqs.(95) and (96). In the figure, γ_o is shown to be constant with height above the surface layer, since $L_w^x/L_u^x = 0.5 =$ a constant. In fact, however, γ_o will decrease as $\overline{uw}/u'w'$ decreases, since, as indicated by Eq. (66), γ_o is proportional to this value.

4.6 Integral Scales

For the planetary layer as a whole, assume $L_v^x = L_w^x$ and the scales L_u^x and L_w^x are given by

$$L_u^x = 20\sqrt{z} \tag{95}$$

and

$$L_w^x = 0.4\ z\ .$$

When the region above the surface layer is being considered alone, the expressions

$$L_u^x = 4.2\ z^{0.73} \tag{96}$$

and

$$L_w^x = 2.1\ z^{0.73}$$

are suggested, and thus in this region, the isotropic relation

$$L_u^x = 2\ L_v^x = 2\ L_w^x$$

is valid.

REFERENCES

1. Bendat, J. S. Piersol, A. G. — Measurement and Analysis of Random Data, Wiley, N.Y., 1966.

2. Hinze, J. O. — Turbulence, McGraw Hill, N.Y., 1959.

3. Sutton, O. G. — Micrometeorology, McGraw Hill, N.Y., 1953.

4. Lumley, J. L. Panofsky, H. A. — The Structure of Atmospheric Turbulence, Wiley, N.Y., 1964.

5. Bowne, N. E. Anderson, G. E. — Take-off and Landing Critical Atmospheric Turbulence, Analytical Investigation, AFFDL-TR-68-23, Wright-Patterson Air Force Base, Ohio, April 1968.

6. Skelton, G. B. — Investigation of the Effects of Gusts on V/STOL Craft in Transition and Hover, AFFDL-TR-68-85, Wright-Patterson Air Force Base, Ohio, October, 1968.

7. Batchelor, G. K. — Homogeneous Turbulence, Cambridge University Press, 1953.

8. Townsend, A. A. — The Structure of Turbulent Shear Flow, Cambridge University Press, 1956.

9. Davenport, A. G. — The Relationship of Wind Structure to Wind Loading, Paper 2, Symp. 16, Proc. of Conf. on "Wind Effects on Buildings and Structures" at NPL in June, 1963. HMSO, London, 1965.

10. Davenport, A. G. — The Dependence of Wind Loads on Meteorological Parameters, Paper 2, Proc. of Int. Symp. on "Wind Effects on Buildings and Structures" at NRC in September, 1967. University of Toronto Press, Toronto, 1968.

11. Davenport, A. G. Isyumov, N. — The Application of the Boundary Layer Wind Tunnel to the Prediction of Wind Loading, Paper 7, IBID.

12. Surry, D. — The Effect of High Intensity Turbulence on the Aerodynamics of a Rigid Circular Cylinder at Sub-critical Reynolds Number, UTIAS Report No.142, October, 1969.

13. Counihan, J. — An Improved Method of Simulating an Atmospheric Boundary Layer in a Wind Tunnel, Atmospheric Environment 3, 1969, pp.197-214.

14. Burns, A. — Power Spectra of Low Level Atmospheric Turbulence Measured from an Aircraft, RAE Tech. Note No. Structures 329, April 1963.

15. Burns, A. — Power Spectra of the Vertical Component of Atmospheric Turbulence Obtained from Concurrent Measurements on an Aircraft and at Fixed Points, RAE Tech.Note No. Structures 325, January 1963.

16. Etkin, B. — Dynamics of Flight: Stability and Control, Wiley, N.Y., 1959.

17. Elderkin, G. E. — Experimental Investigation of the Turbulence Structure in the Lower Atmosphere, Batelle-Northwest Report 329, Pacific Northwest Laboratory, Richland Washington, December 1966.

18. Payne, F. R.; Lumley, J. L. — One-Dimensional Spectra Derived from an Airborne Hot-Wire Anemometer, Qu. J. Roy. Met. Soc., 92, No.393, July 1966.

19. Lappe, U. O.; Davidson, B.; Notess, C. B. — Analysis of Atmospheric Turbulence Spectra Obtain from Concurrent Airplane andTower Measurements, IAS Report No.59-44, January 1959.

20. Saunders, K. D. — B-66B Low Level Gust Study, Vol.1, WADD Tech. Report 60-305, Wright-Patterson Air Force Base, Ohio, March 1961.

21. Notess, C. B. — Analysis of Turbulence Data Measured in Flight at Altitudes up to 1600 feet Above Three Different Types of Terrain, Cornell Aero. Lab. Report No. TE-1215-F-1, April 1959.

22. Wardlaw, R. L.; Davenport, A. G. — Some Experiments on the Fluctuating Forces on Flat Plates in Turbulent Flow, NRC Aero. Report LR 416, December 1964.

23. Blackadar, A. K. — The Vertical Distribution of Wind and Turbulent Exchange in a Neutral Atmosphere, Jour. Geophys. Research, Vol.87, No.8, July 1962.

24. Panofsky, H. A. — Scale Analysis of Atmospheric Turbulence at 2m., Qu. J. Roy. Met. Soc., 88, 1962, pp.57-69.

25. Grant, H. L. — The Large Eddies of Turbulent Motion, J. Fluid Mech., 4, 1958, pp. 149-190.

26. Henry, R. M. — A Study of the Effects of Wind Speed, Lapse Rate, and Altitude on the Spectrum of Atmospheric Turbulence at Low Altitude, IAS Report No.59-43, January 1959.

27. Houbolt, J. C.; Steiner, R.; Pratt, K. G. — Dynamic Response of Airplanes to Atmospheric Turbulence Including Flight Data on Input and Response, NASA TR R-199, June 1964.

28. Lappe, U. O. — A Low Altitude Gust Model for Estimating Gust Loads on Aircraft, AIAA Paper 65-14, January 1965.

29. Panofsky, H. A.; McCormack, R. A. — The Spectrum of Vertical Velocity Near the Surface, IAS Report No.59-6, January 1959.

30. Templin, R. J. — Interim Progress Note on Simulation of Earth's Surface Winds by Artificially Thickened Wind Tunnel Boundary Layers, National Research Council of Canada, NAE Report LTR-LA-22, February 1969.

31. Davenport, A. G. — The Buffeting of Large Superficial Structures by Atmospheric Turbulence. Reprinted from the Annals of the New York Academy of Sciences, Vol.116, Article 2, June 1964, pp.135-159.

32. van der Hoven, I. — Power Spectrum of Horizontal Wind Speed in the Frequency Range from 0.0007 to 900 Cycles Per Hour,J. Meteor., 14, April 1957, pp.160-164.

33. Panofsky, H. A. — A Survey of Recent Ideas on Low Level Atmospheric Turbulence, Symp. on the Theory and Meas. of Atmos. Turbulence and Diffusion in the Planetary Boundary Layer. Reprint, Sandia Laboratories, SC-M-67-2931, 1967.

34. Panofsky, H. A.; Townsend, A. A. — Change of Terrain Roughness and the Wind Profile, Qu. J. Roy. Met. Soc., 90, 1964, pp.147-155.

35. Panofsky, H. A.; van der Hoven, I. — Spectra and Cross-Spectra of Velocity Components in the Meso-Meteorological Range, Qu. J. Roy. Met. Soc., 81, 1955, pp.603-606.

36. Campbell, G. S.; Standen, N.M. — Progress Report II on Simulation of Earth's Surface Winds by Artificially Thickened Wind Tunnel Boundary Layers, National Research Council of Canada, NAE Report LTR-LA-37, July 1969.

37. Davenport, A. G. — The Spectrum of Horizontal Gustinesss Near the Ground in High Winds, Qu. J. Roy. Met. Soc., 87, April 1961, pp.194-211.

38. Lappe, U. O.; Davidson, B. — On the Range of Validity of Taylor's Hypothesis and the Kolmogoroff Spectral Law, J. Atmos. Sci., 20, November 1963, pp.569-576.

39. Fichtl, G. H.; McVehil, G. E. — Longitudinal and Lateral Spectra of Turbulence in the Atmospheric Boundary Layer, NASA TN D-5584, February 1970.

40. Berman, S. — Estimating the Longitudinal Wind Spectrum Near the Ground, Qu. J. Roy. Met. Soc., 91, 1965, pp.302-317.

41. Busch, N. E.; Panofsky, H. A. — Recent Spectra of Atmospheric Turbulence, Proc. Unguided Rocket Ballistics Meteorology Conference, New Mexico State University 1967, pp.215-257.

42. Davenport, A. G. — Rationale for Determining Design Wind Velocities, J. Struct. Div., Proc. Amer. Soc. Civil Eng., May 1960.

43. Gunter, D. E.; Jones, G. W.; Jones, J. W.; Monson, K. R. — Low Altitude Atmospheric Turbulence, Lo-Locat Phases 1 & 11, ASD-TR-69-12, Wright-Patterson Air Force Base, Ohio, February 1969.

44. Panofsky, H. A. — Determination of Stress From Wind and Temperature Measurements, Qu. J. Roy. Met. Soc., 89, 1963, pp.85-94.

45. Panofsky, H. A. — The Relation Between Eulerian Time and Space Spectra, Qu. J. Roy. Met. Soc., 84, 1958, pp.270-273.

46. Faller, A. J. — Large Eddies in the Atmospheric Boundary Layer and Their Possible Role in the Formation of Cloud Rows, J. Atmos. Sci., 22, March 1965, pp.176-184.

47. Townsend, A. A. — Natural Convection in the Earth's Boundary Layer, Qu. J. Roy. Met. Soc., 88, 1962, pp.51-56.

48. Webb, E. K. — Autocorrelations and Energy Spectra of Atmospheric Turbulence, C.S.I.R.O. Div. Met. Phys. Tech. Paper No.5, Melbourne, Australia, 1955.

49. Stewart, R. W. — A New Look at the Reynolds Stresses, Can. J. Phys., 34, 1959, pp.722-725.

50. Pritchard, F. E. — A Statistical Model of Atmospheric Turbulence and a Review of the Assumptions Necessary for Its Use, Presented at the AGARD Specialists Meeting on Stability and Control, Cambridge, England, September 1966.

51. Taylor, J. — Manual on Aircraft Loads, AGARDograph 83, Pergamon Press, 1965.

52. Singer, I. A. — Wind Gust Spectra, N.Y. Acad of Sci. Vol.116, Art. 1, pp. 116-133, June 1964.

53. Case, E. R.; Maritan, P. A.; Gorjup, M. — Development of a Low Altitude Gust Model and Its Application to STOL Aircraft Response Studies, de Havilland Aircraft of Canada, DHC-DIR 68-15, May 1969.

54. Favre, A. J. — Review on Space-Time Correlations in Turbulent Fluids, Transactions of ASME, J. App. Mech., 1965.

55. Lin, C. C. — On Taylor's Hypothesis and the Acceleration Terms in the Navier-Stokes Equations, Qu. App. Math., 10, 1953, pp.295-306.

56. Lumley, J. L. — The Spectrum of Nearly Inertial Turbulence in a Stably Stratified Fluid, J. Atmos. Sci., 21, January 1964, pp.99-102.

57. Joppa, R. G. — A Proposed Model of Low Altitude Atmospheric Turbulence for Use in V/STOL Aircraft Handling Qualities Studies, Boeing Co. 02A BC.R-AD 059570, Document No.DG-10 38, February 1965.

58. Harris, R. I. — The Nature of the Wind, Presented at the Construction Industry Research and Information Association Seminar on the Modern Design of Wind-Sensitive Structures at London, England, June 18, 1969.

59. Cramer, H. E.
Record, F. A.
Tillman, J. E.
Studies of the Spectra of the Vertical Fluxes of Momentum, Heat, and Moisture in the Atmospheric Boundary Layer, Final Report DA Task 3A 99-27-005-08, Contract No.DA-36-039-SC-80209, Meteorological Department, Mass. Inst. of Tech., April 1962.

60. Klebanoff, P. S.
Characteristics of Turbulence in a Boundary Layer with Zero Pressure Gradient, NACA Report 1247, 1955.

61. Schlichting, H.
Boundary Layer Theory, McGraw Hill, N.Y., 1955.

62. Harris, R. I.
On the Spectrum and Auto-Correlation Function of Gustiness in High Winds, E.R.A. Tech. Rep. 5273, Leatherhead, England, 1968.

63. Panofsky, H. A.
The Structure of Atmospheric Shear Flows, Paper 1, Ref.66.

64. Cermak, J. E.
Arya, S.P.S.
Problems of Atmospheric Shear Flows and Their Laboratory Simulation, Paper 12, Ref.66.

65. Harris, R. I.
Measurements of Wind Structure at Heights up to 598 ft. Above Ground Level, E.R.A. Tech. Rept. 5258, Leatherhead, England, 1968.

66.
Aerodynamics of Atmospheric Shear Flows, AGARD Conference Proceedings No.48, February 1970.

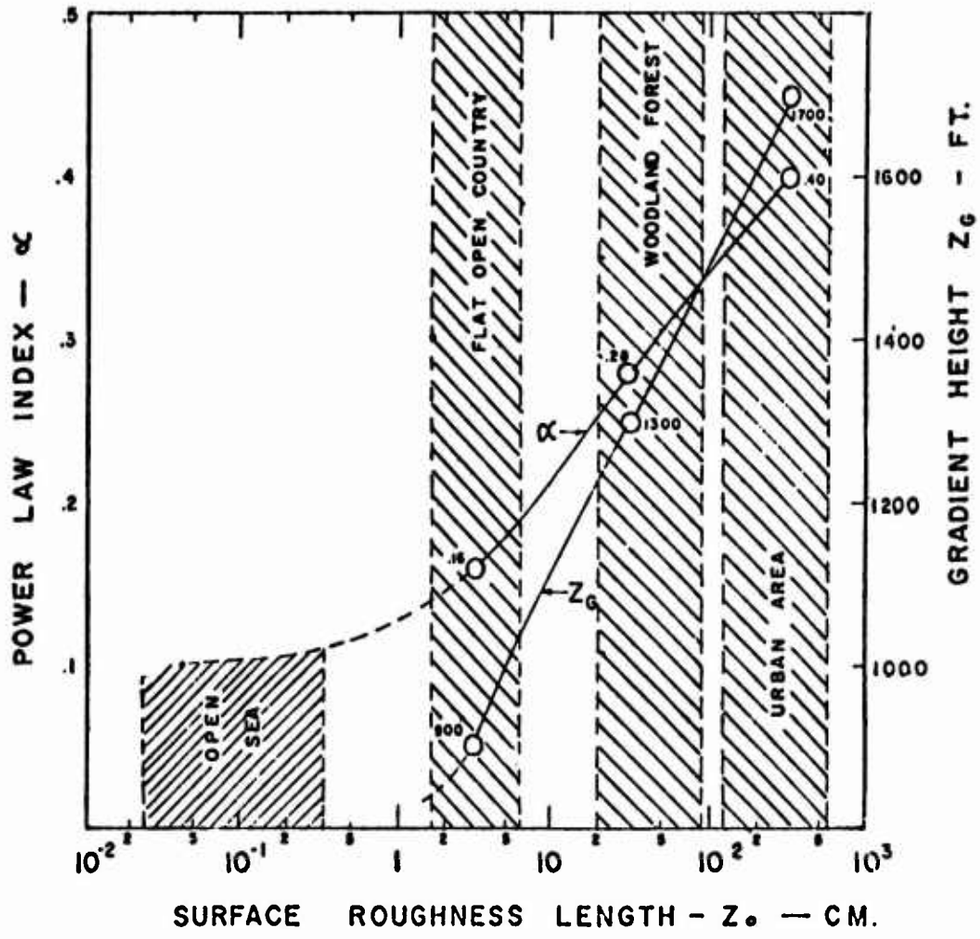

FIG. 1 PARAMETERS OF THE POWER LAW
FOR MEAN WIND VELOCITY (FROM REF. 9)

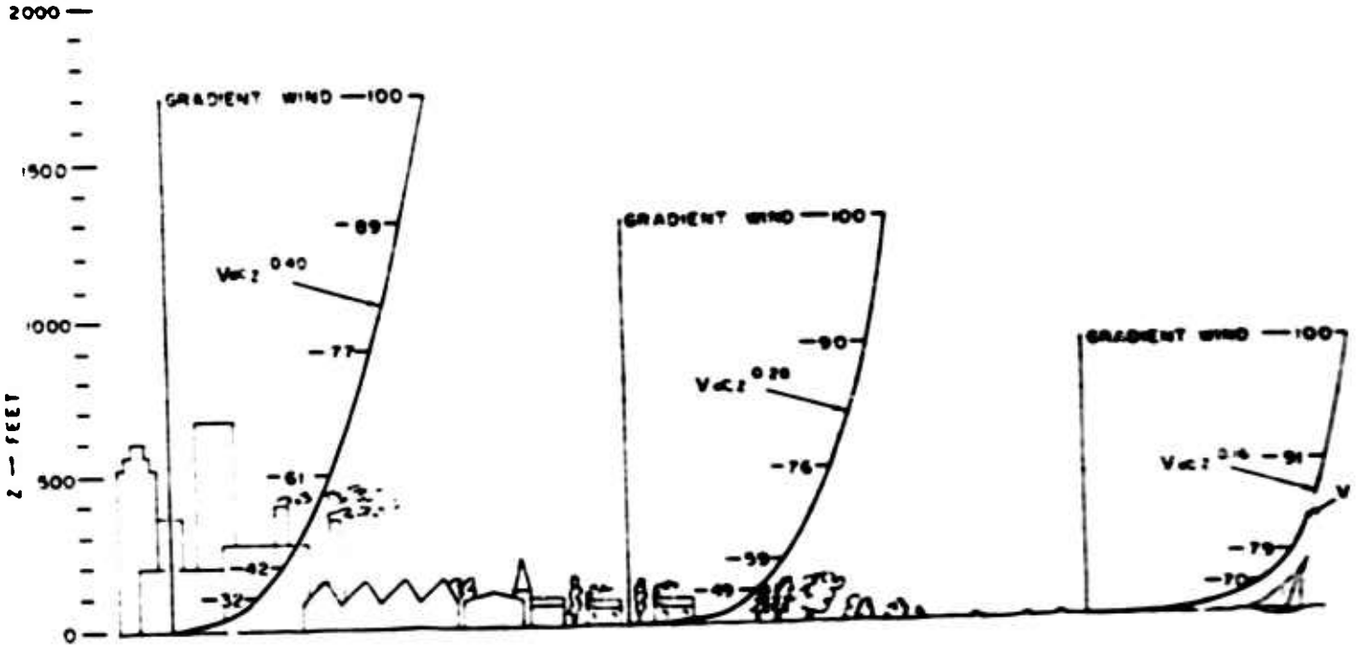

FIG. 2 TYPICAL MEAN WIND PROFILES OVER UNIFORM TERRAINS OF DIFFERING ROUGHNESS (FROM REF. 9)

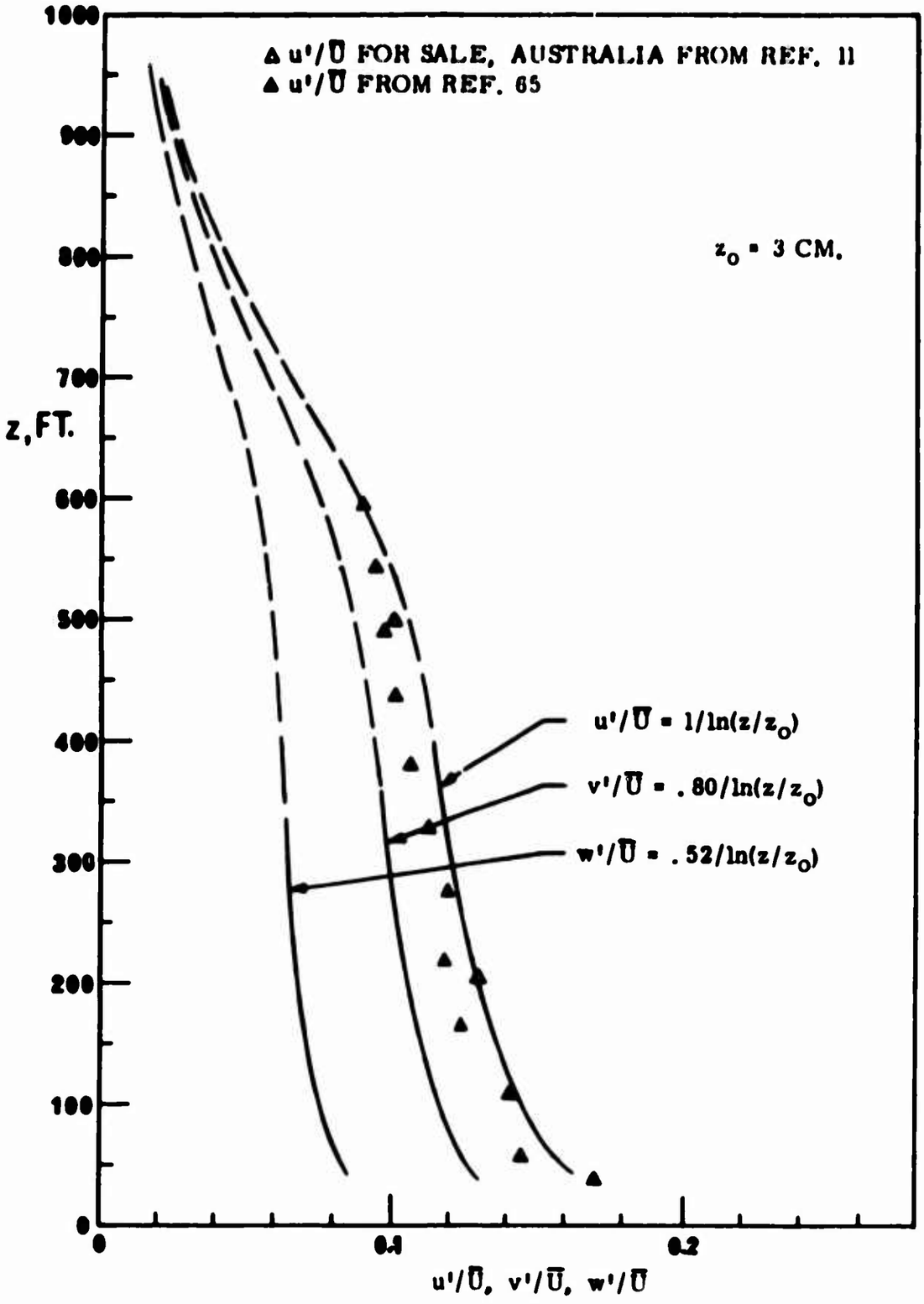

FIG. 3 TURBULENCE INTENSITY VARIATION WITH HEIGHT IN NEUTRAL STABILITY OVER FLAT TERRAIN

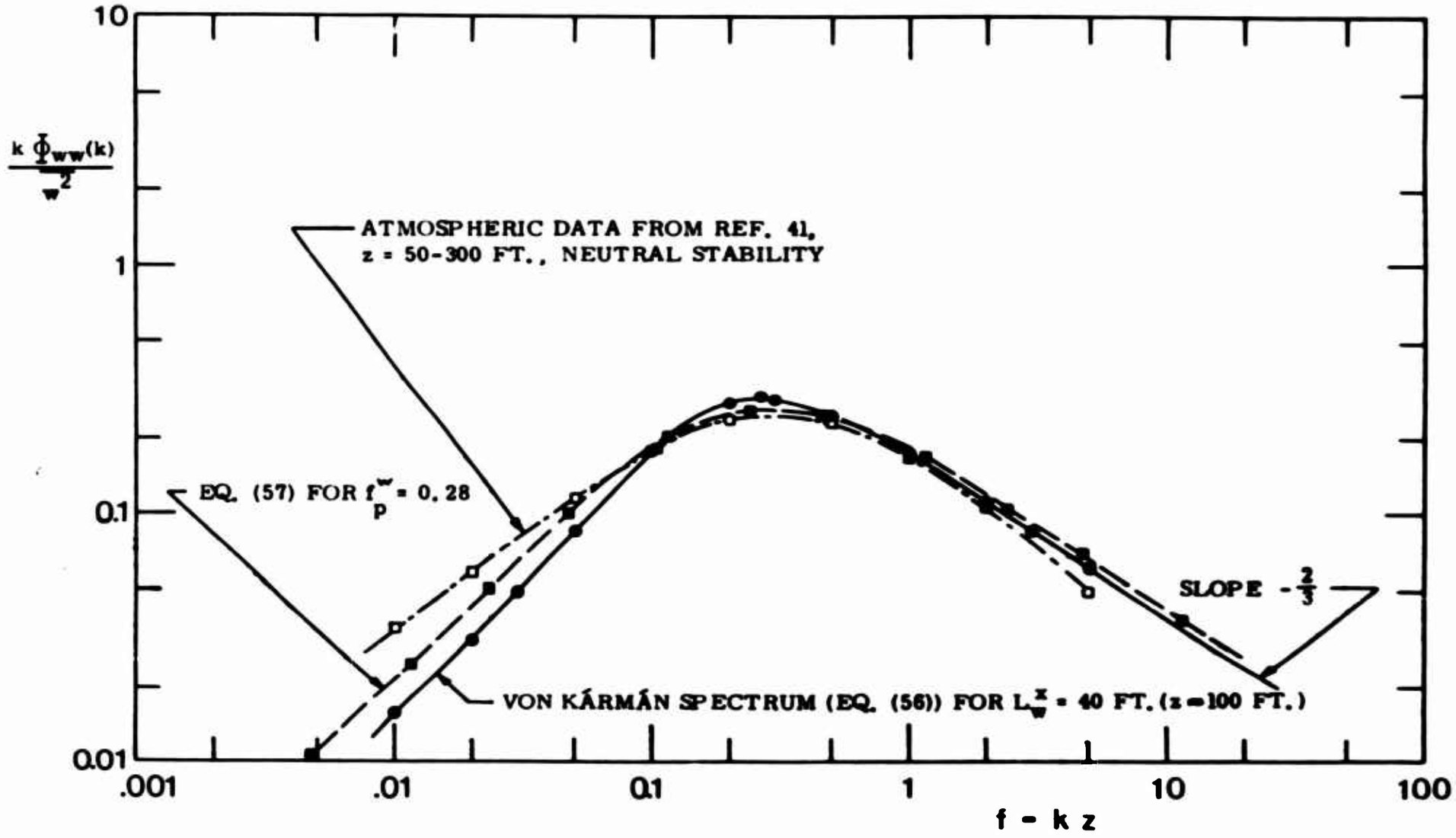

FIG. 4 VERTICAL COMPONENT POWER SPECTRA IN THE SURFACE LAYER

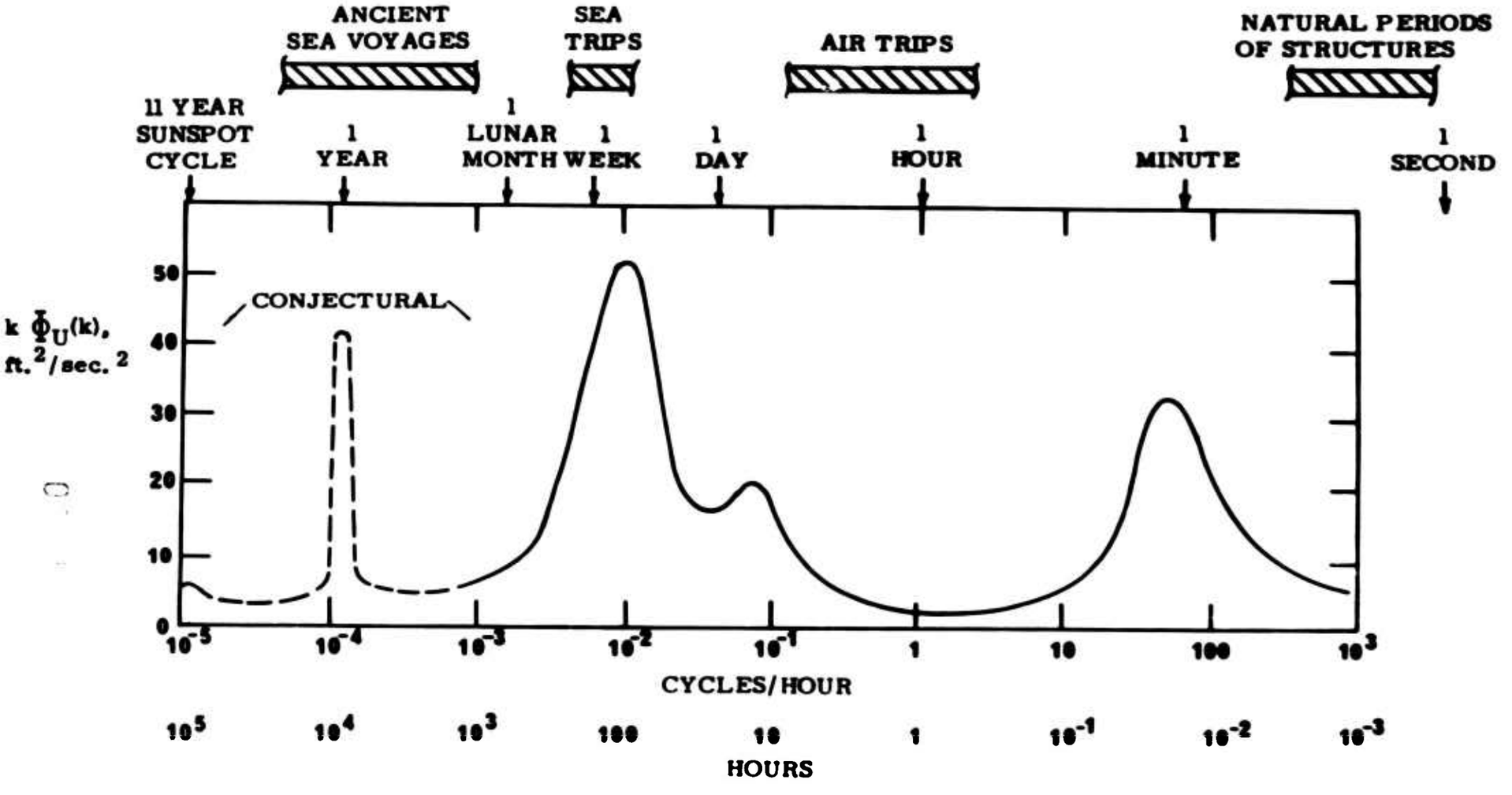

FIG. 5 SPECTRUM OF WIND SPEED AT BROOKHAVEN, U. S. A. (FROM REF. 30)

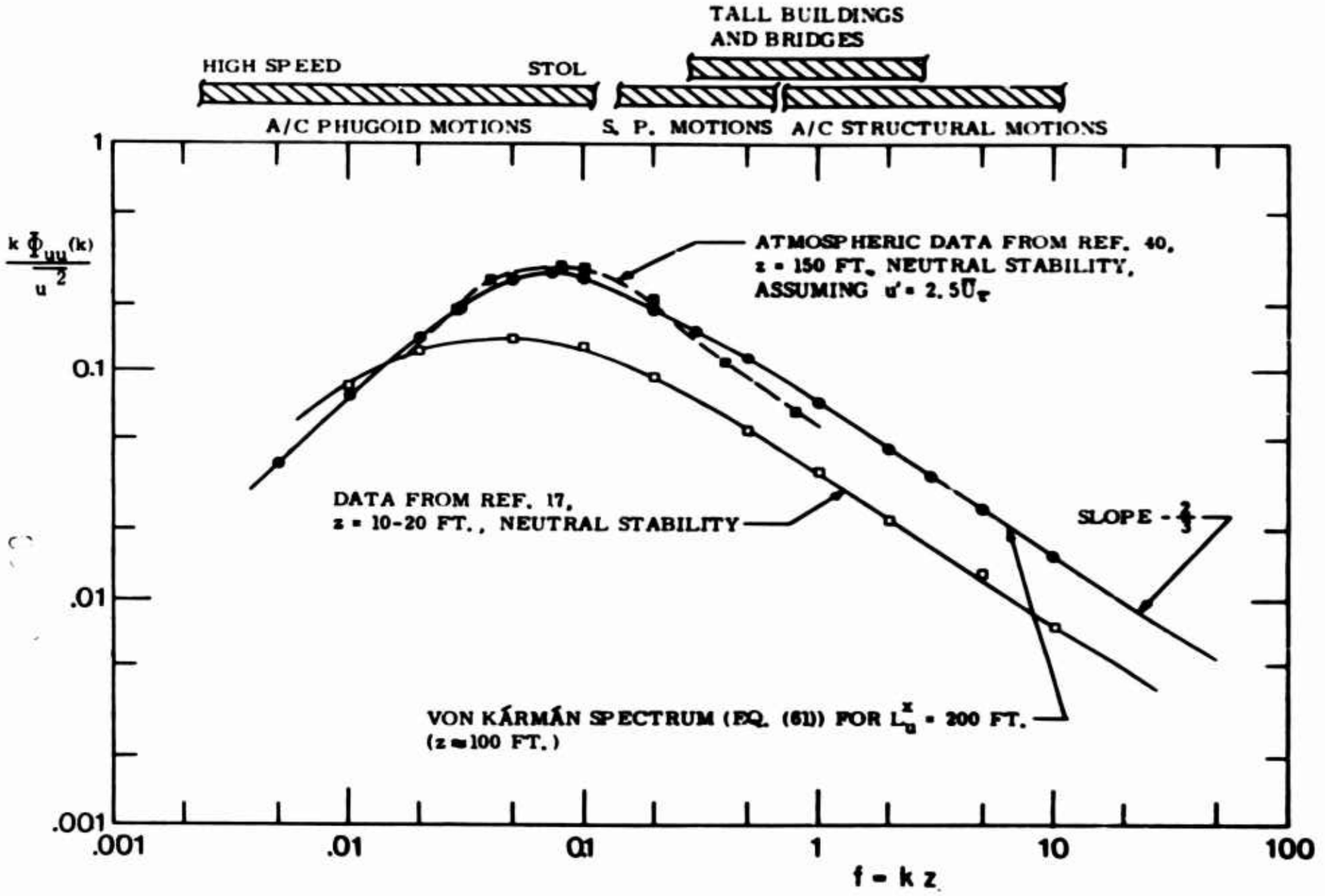

FIG. 5 LONGITUDINAL COMPONENT POWER SPECTRA IN THE SURFACE LAYER

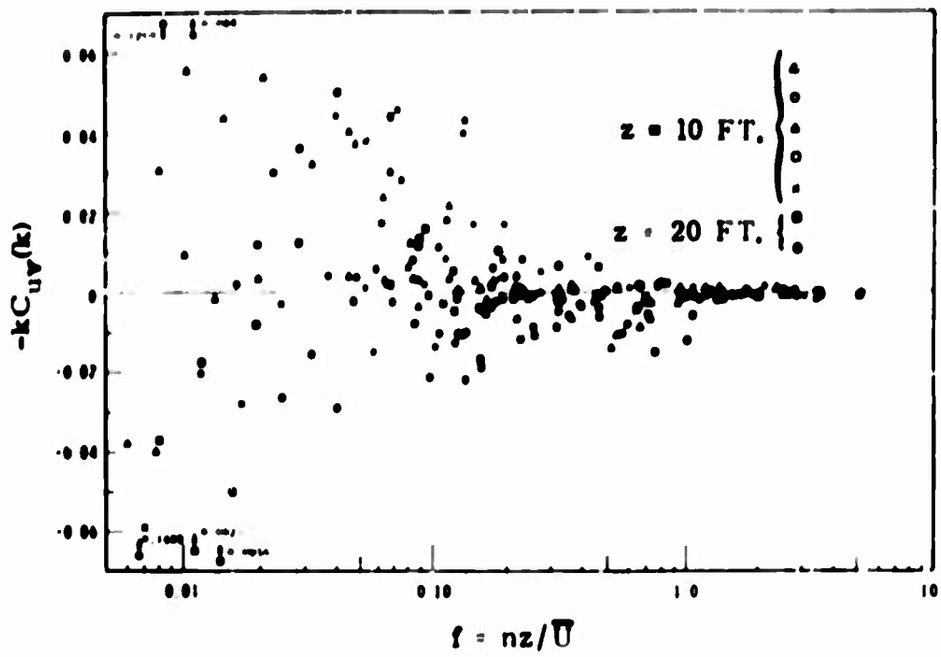

FIG. 7 COSPECTRA BETWEEN LONGITUDINAL AND LATERAL VELOCITY-NEUTRAL STABILITY

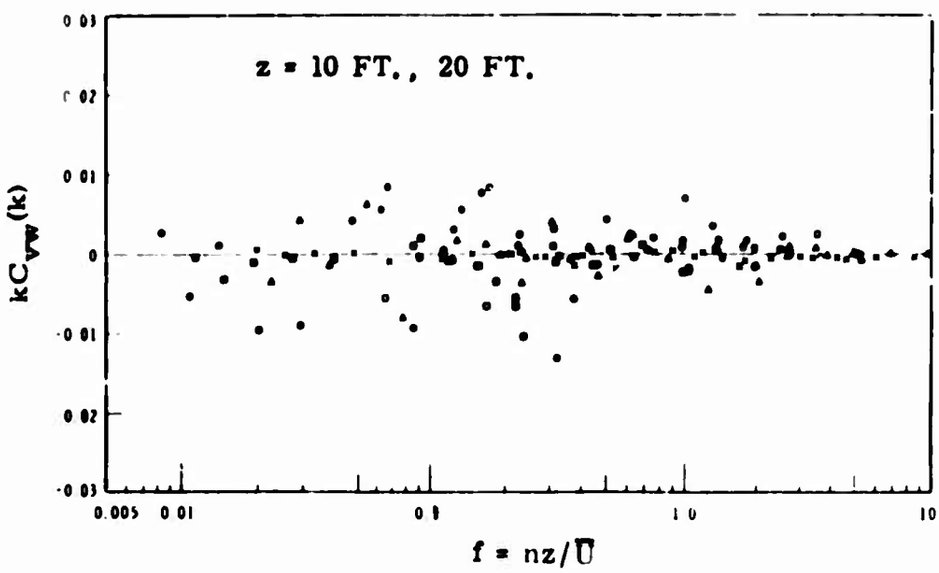

FIG. 8 COSPECTRA BETWEEN LATERAL AND VERTICAL VELOCITY-STABLE AIR

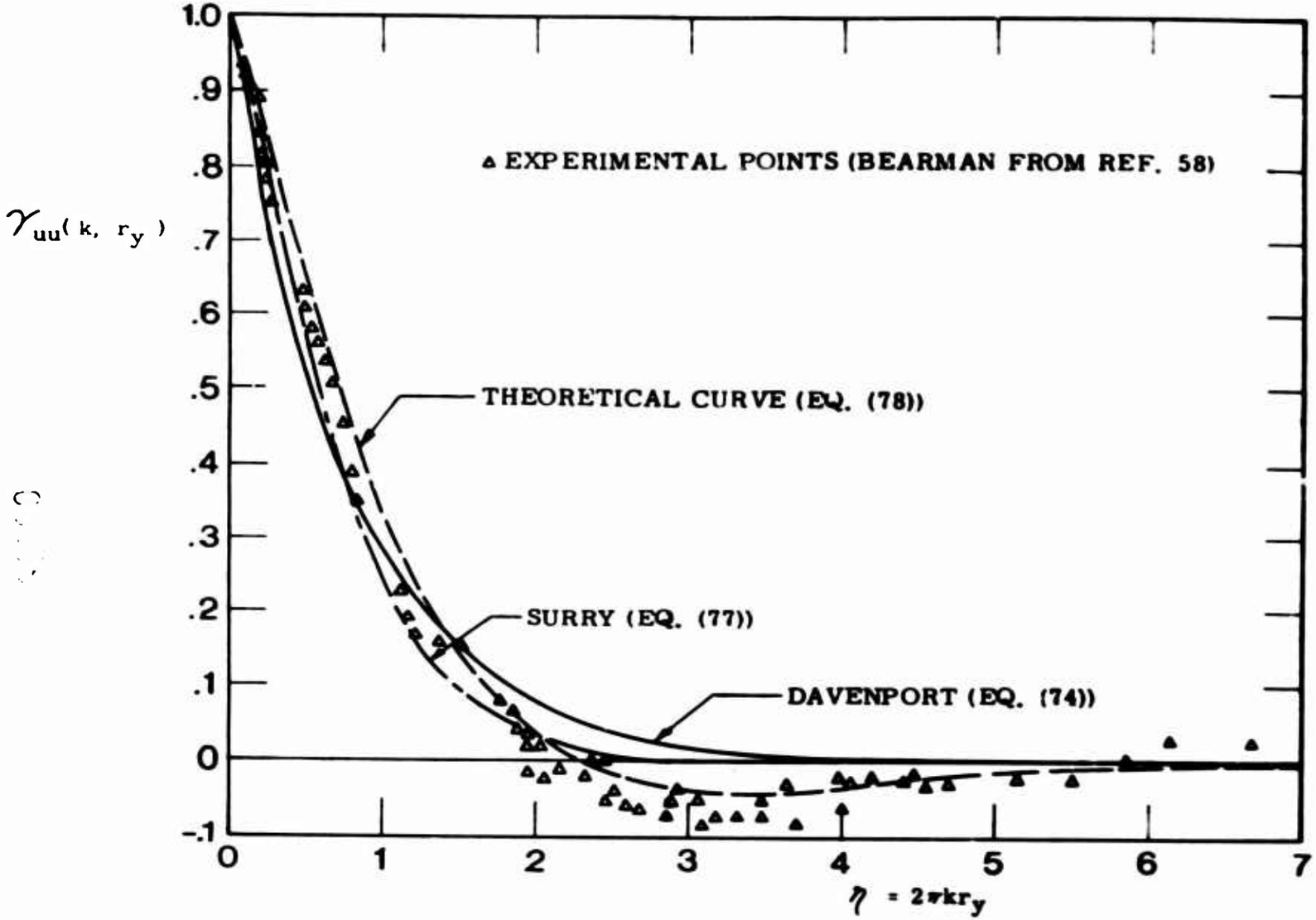

FIG. 9 CROSS-CORRELATION SPECTRA FOR GRID-GENERATED TURBULENCE

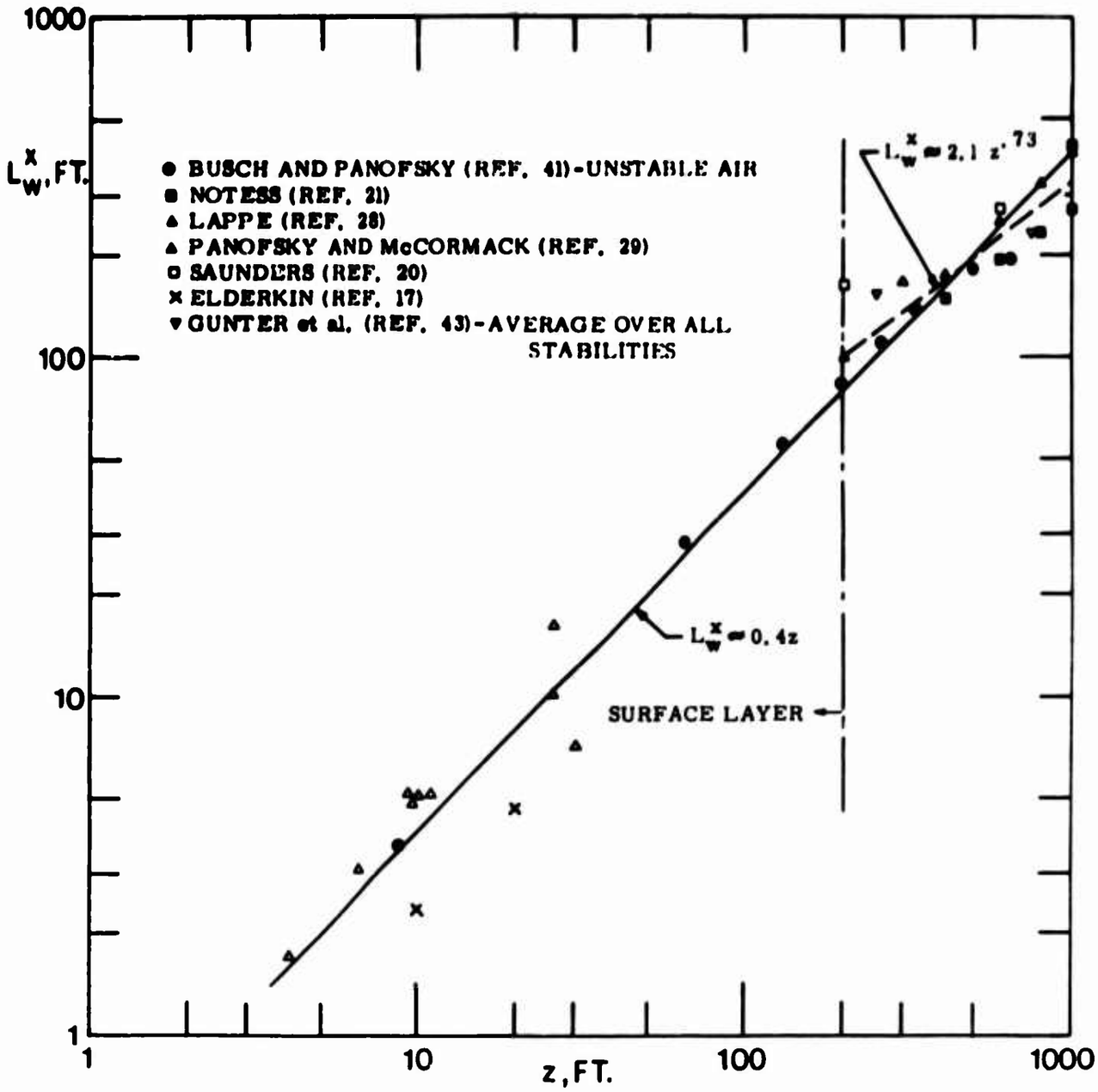

FIG. 10 VERTICAL COMPONENT SCALE VARIATION WITH HEIGHT IN NEUTRAL STABILITY OVER FLAT TERRAIN

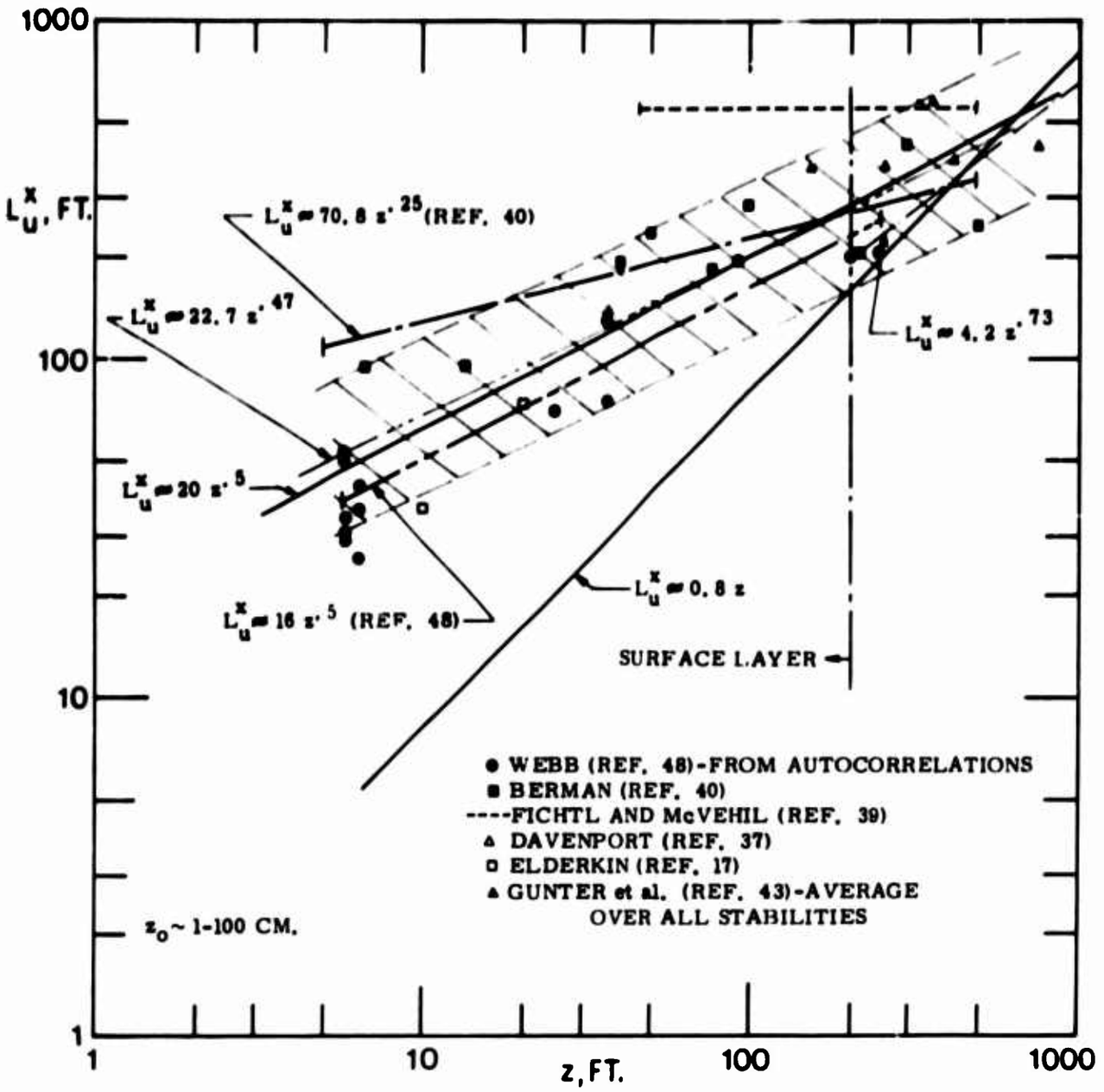

FIG. 11 LONGITUDINAL COMPONENT SCALE VARIATION WITH HEIGHT IN NEUTRAL STABILITY OVER FLAT TERRAIN

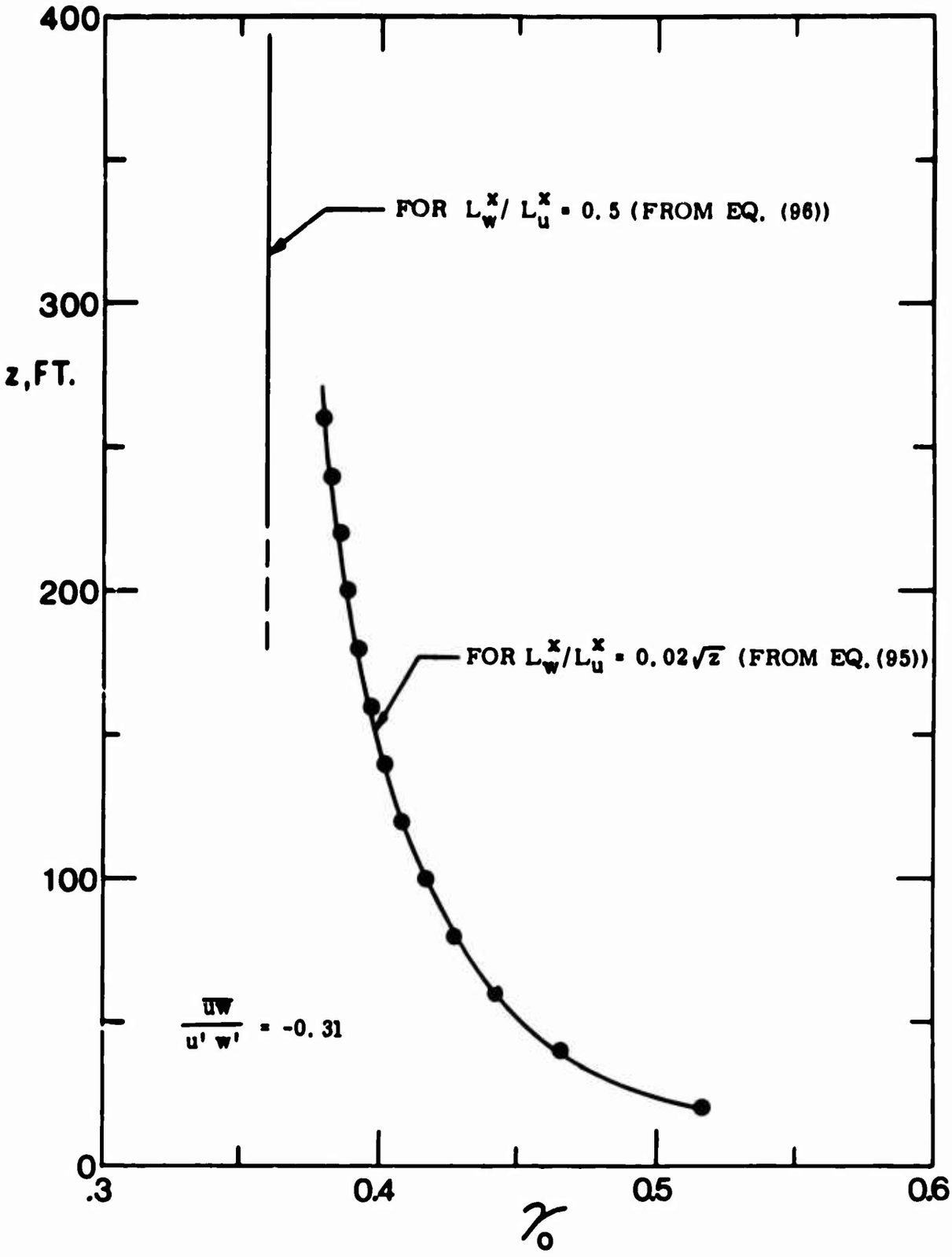

FIG. 12 VARIATION OF γ_0 WITH HEIGHT FOR MATHEMATICAL MODEL